16
FALL ISSUE

AIRCRAFT SURVIVABILITY

published by the
Joint Aircraft
Survivability
Program Office

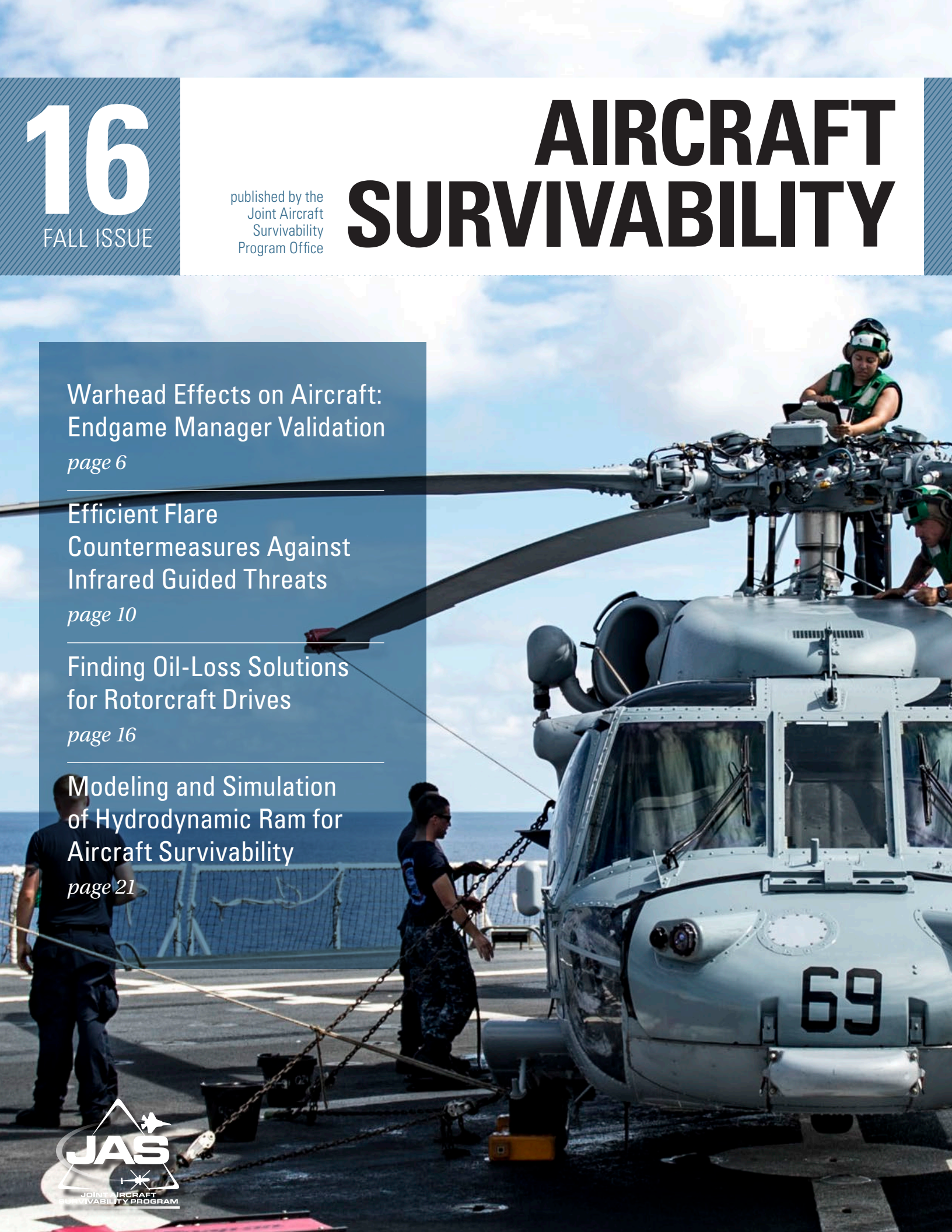

JAS
JOINT AIRCRAFT SURVIVABILITY PROGRAM

Aircraft Survivability is published three times a year by the Joint Aircraft Survivability Program Office (JASPO), chartered by the U.S. Army Aviation & Missile Command, U.S. Air Force Life Cycle Management Center, and U.S. Navy Naval Air Systems Command.

JAS Program Office
735 S. Courthouse Road
Suite 1100
Arlington, VA 22204-2489
http://jasp-online.org/

Sponsor
Dennis Lindell

Editor-in-Chief
Dale Atkinson

Views and comments may be directed to the JAS Program Office.

To order back issues of the *AS Journal,* send an email to ***contact@dsiac.org***

On the cover:
Sailors conduct maintenance on an MH-60S helicopter on the flight deck of hospital ship USNS Mercy. (U.S. Navy photo)

TABLE OF CONTENTS

Since childhood, aircraft dog fights have captured many of our imaginations. Even for those of us who have not seen actual combat, Hollywood movies have put us inside cockpits to experience the gut-wrenching drama of an enemy missile heading our way, the wailing missile warning alarm, and the pilot's deployment of countermeasures immediately followed by a HARD high-g turn. But these pilot actions are not accidental. In actual combat, the outcomes of such events are influenced by tactics, techniques, and procedures (TTPs) that dictate countermeasure execution and timing in sequence with flight maneuvers. Simply put, TTPs are critical operational instructions by which U.S. military pilots fly, fight, and win. In addition, TTP viability and effectiveness are judged through flight tests supplemented by exhaustive modeling and simulation (M&S).

Portable infrared (IR) guided missiles have been the biggest threat to aircraft, especially low-speed helicopters, for the last several decades. The development of IR-based seekers for missile guidance has been an especially active research field, resulting in various emerging and/or advanced technologies, such as spin scan, conical scan, Rosetta scan, and image seekers [1]. Likewise, numerous aircraft countermeasures (CMs) against these threats, including flares, infrared countermeasures (IRCM), and directed infrared countermeasures (DIRCM), have been developed. And as aircraft have had countermeasuring equipment installed, the seekers have adopted infrared counter-countermeasures (IRCCM).

Mailing list additions, deletions, changes, as well as calendar items may be directed to:

DSIAC
Defense Systems Information Analysis Center

DSIAC Headquarters
4695 Millennium Drive
Belcamp, MD 21017-1505
Phone: 443/360-4600
Fax: 410/272-6763
Email: *contact@dsiac.org*

DSIAC is sponsored by the Defense Technical Information Center (DTIC) and is operated by the SURVICE Engineering Company under Contract FA8075-14-D-0001.

DSIAC Program Manager
Ted Welsh

Production Editor
Eric Edwards

Art Director
Melissa Gestido

Distribution Statement A: Approved for public release; distribution unlimited, per DoD Office of Prepublication and Security Review, Case No. 16-S-2581.

NEWS NOTES

By Dale Atkinson

The aircraft survivability community has lost a pioneer in the field of survivability and lethality simulation. On 25 February 2016, Earl E. Wilhelm passed away at the age of 86. Earl was born on 5 September 1927 in Okmulgee, OK. He graduated from the University of Oklahoma, achieving a master's degree in engineering physics. He began his career as a research specialist at the Boeing Company in 1964, initially becoming a specialist in weapon lethality and participating in warhead design and testing, where he was granted five patents. His talents eventually progressed to aircraft survivability with his transition to aircraft vulnerability assessments. He became an expert in FASTGEN/COVART analyses and was a regular participant in the Joint Aircraft Survivability Program Office (JASPO) Model Users Meetings (JMUM). In 1998, Earl was recognized by the Boeing Company as an Associate Technical Fellow (ATF). He retired from Boeing in 2013 with 48 years of service. He is survived by his wife, Chien-Chiu; his three children, Steve, Thomas, and Key; his stepson, Chi-Ju; and his granddaughter, Ella. Earl and his longstanding participation in the weapon system analysis community will be greatly missed. ASJ

JCAT CORNER

by Maj. Ron Pendleton, CW5 Mike Apple, and CAPT. David Storr

The Joint Combat Assessment Team (JCAT), consisting of Army, Navy, and Air Force contingents, continues to adapt to the ever-changing worldwide operations to process evidence from aircraft hostile fire incidents and give combatant aircraft unit commanders immediate threat data, while also providing data for engineering improvements to reduce the loss of lives and aircraft.

Since the withdrawal of the forward-deployed JCAT assessors in late 2014, we all have pursued alternate means to collect hostile fire damage data. For U.S. Air Force (USAF) JCAT, one source of these data is the aircraft battle damage reports submitted by deployed aircraft maintenance units. Another source is via increasing the working relationships with deploying depot liaison engineers. These active duty engineers operate downrange on a rotating basis, supporting maintenance units with aircraft repairs that exceed the published tech order limits. These individuals also reach back to structures engineering offices at the stateside air logistics bases to design and substantiate structural repairs for all aircraft types. They are also trained in aircraft battle damage repair engineering, which is a valued experience factor for the combat forensic work of JCAT. Two depot liaison engineers were selected for, and have completed, the 2016 JCAT training curriculum.

JCAT Phase 3, the Threat Weapons Effects (TWE) training, is conducted by a different Service each year, and this year was the USAF's turn. The event was conducted at the King Auditorium at Hurlburt Field as well as at locations in the Hurlburt/Eglin AFB complex. Approximately 200 personnel attended, including military and civilians in the survivability, intelligence, and aircraft operation fields. Subject-matter experts delivered briefings on various topics, such as design for combat rescue helicopter aircraft survivability; recent hostile fire events; man-portable air defense systems (MANPADS) cueing using commercial-off-the-shelf (COTS) technology; specificity in survivability requirement language; Bureau of Alcohol, Tobacco, Firearms and Explosives (ATF) trends in explosives; forensic collection techniques; warhead design and blast effects; air-to-air threats; anti-tank guided missile threats

Figure 1 DIT Demo at the 2016 TWE

Figure 2 DIT Demo at the 2016 TWE

to aircraft; and KC-46 ballistic and long-duration burn tests.

And back by popular demand, this year's TWE featured the Dynamics of International Terrorism (DIT) demonstration (as shown in Figures 1 and 2). It has been four years since TWE included the much-enjoyed demo, which is a live demonstration of the tactics and effects of terrorist enemy weapons, ranging from Molotov cocktails to improvised explosive devices (IEDs) to automatic small arms against a variety of targets, such as armor plating, vehicles, and human analogs.

Attendees also enjoyed several tour opportunities, such as the Seekers & Sensors (Open Air & Seeker Test Van) Laboratory, Electronic Design & Fabrication Laboratory, Joint Preflight Integration of Munitions and Electronic Systems (J-PRIMES) Test Facility, Foreign Targets Compound (formerly called Chicken Little), and the McKinley Climactic Laboratory.

With the end of another successful TWE, efforts to plan and coordinate next year's event have begun. The Navy JCAT falls under the NAVAIRSYSCOM Navy Reserve Unit – NR NAVAIR In Service Engineering and Logistics (ISEL) and has the responsibility to organize, coordinate, and host next year's event. The 2017 TWE Seminar is scheduled for 2–4 May in Fort Walton Beach, FL. The theme is Emerging Threats, and the 3-day briefing will cover threats that are of primary concern to Department of Defense (DoD) rotary- and fixed-wing aircraft.

In addition to planning the 2017 TWE Seminar, Navy Reserve ISEL Detachment Bravo has been coordinating an upcoming Live Fire Test and Evaluation (LFT&E) event to take place at Naval Air Warfare Center – Weapons Division, China Lake, CA. The LFT&E event is sponsored by the Joint Aircraft Survivability Program Office (JASPO) and is designed to demonstrate the weapons effects of a "red" surface-to-air missile (SAM) against a U.S. fixed-wing aircraft. The warhead has been acquired from the Missile and Space Intelligence Center (MSIC) and will be shipped to the Naval Air Weapons Station (NAWS) China Lake via the Navy Air Logistics Office (NALO). Navy JCAT will rely on this live-fire scenario to demonstrate a threat SAM engagement against a currently operating fixed-wing airframe. Additional flight control surfaces, fuel tanks, and aircraft systems will be staged in the vicinity of the detonation to serve as witness plates to take advantage of this unique LFT&E opportunity. Once complete, a thorough analysis and assessment will be conducted, and the results will be documented and used to train future JCAT assessors and provide survivability engineers data to support threat mitigation to future DoD aircraft and aircraft systems.

The Army JCAT team remains busy keeping up with the ongoing events downrange, conducting assessments, and uploading the results into the Combat Damage Incident Reporting System (CDIRS) database on a regular basis. Along with conducting assessments, the team continues to brief the students who come through the Professional Military Education (PME) courses at Fort Rucker, AL, and travel to unit locations to conduct unit briefs and pre-deployment briefs. With the current operations pace, the team is on par to brief more than 4,000 personnel this year. These briefs keep the aviation community aware of the efforts of the JASP and JCAT programs, emerging worldwide threats, and current tactical events.

Article continued on page 9

WARHEAD EFFECTS ON AIRCRAFT: ENDGAME MANAGER VALIDATION

by Greg Czarnecki, Ron Schiller, Mitch Shedden, and John Haas

Figure 1 Instrumented Aircraft with Missile Test Stand in Place

Since childhood, aircraft dog fights have captured many of our imaginations. Even for those of us who have not seen actual combat, Hollywood movies put us inside cockpits to experience the gut-wrenching drama of an enemy missile heading our way, the wailing missile warning alarm, and the pilot's deployment of countermeasures immediately followed by a HARD high-g turn. But these pilot actions are not accidental. In actual combat, the outcomes of such events are influenced by tactics, techniques, and procedures (TTPs) dictating countermeasure execution and timing in sequence with flight maneuvers. Simply put, TTPs are critical operational instructions by which U.S. military pilots fly, fight, and win. In addition, TTP viability and effectiveness are judged through flight tests supplemented by exhaustive modeling and simulation (M&S).

At the end of the M&S chain is Endgame Manager. Endgame Manager's role is to assess the final outcome of engagements where missiles get a little too close. Endgame Manager assessments have to be correct to assure TTP credibility and the greatest probability of aircraft and pilot survival.

At the request of the Air Force Life Cycle Management Center (AFLCMC) and by direction of the Director of Operational Test & Evaluation (DOT&E) and the Joint Live Fire (JLF) Program, the 96th Test Group (96 TG) and the Naval Air Warfare Center (NAWC) for Weapons Development joined forces to verify Endgame Manager credibility for aggressive missile-aircraft engagement scenarios. The 96 TG (supported by Skyward Ltd.) assumed overall project leadership, including responsibilities for test planning, test design assistance, test guidance, early damage assessments, data analysis, and reporting. NAWC's

responsibilities included missile and aircraft test asset provisioning, test design, and test execution. Significant technical contributions were also provided by AFLCMC (including test design assistance and pretest predictions), the Joint Combat Assessment Team (JCAT) and the 388th Aircraft Maintenance Squadron (AMXS) (which provided post-test damage investigation, including estimates of damage effects on the aircraft operation), and a weapons program office (which provided test hardware and test design guidance). Together, this team performed warhead-aircraft tests and assessments necessary to verify the credibility of Endgame Manager.

TEST SCENARIOS

While fully realistic scenarios include the relative motion of both missile and aircraft, an initial assumption was that Endgame Manager credibility could be assessed via a static ground test. (Missile-aircraft velocity vectoring within Endgame Manager was already understood as accurate.) To this end, the test design process began. The team selected an F-16 as the target aircraft based on the availability of full-up aircraft test hardware and a detailed aircraft geometry model. The team also selected warhead types/sizes and engagement conditions to provide challenging conditions for Endgame Manager. Primary warhead-selection factors included blast yield and fragment size/count. Engagement conditions (missile-aircraft orientations and separation distances) were selected to adhere with expected encounter scenarios and to produce tests that caused significant, but noncatastrophic, combined blast/fragmentation damage to the aircraft.

Team members considered several test design concepts before settling on two test scenarios that involved missiles with similar fragment types but different explosive yields. Each test would have the warhead (complete with surrogate fore and aft bodies) detonated while stationary above the aircraft. Blast and fragment spray for Test #1 would be directed toward the aircraft's aft right quarter. That for Test #2 would be directed toward the forward left quarter. Separating the damage zones prevented ambiguities of test results, allowed rapid back-to-back tests, and reduced range time/cost.

AFLCMC used Endgame Manager to assist in test design by ensuring that engagement paths and interactions were representative of expected conditions and that resulting damage would provide useful V&V data. The burst point location was determined by using Endgame Manager's fuzing methodology in conjunction with trajectories provided by the weapons program office. Endgame Manager's Forced Miss mode used the velocity vector and orientation for both target and threat along with horizontal and vertical miss distances to calculate a burst point. Endgame Manager then sent the threat down its trajectory containing the Point of Closest Approach (PCA). The burst point derived from Endgame Manager matched the PCA generated by weapons program office data with some offset due to the threat-specific fuze delay. This offset was used to ensure testing at a burst point that produced useful data (i.e., a significant amount of warhead fragment hits, but not so many that the aircraft was completely devastated). Once representative missile-aircraft positions/orientations were identified and locked in, AFLCMC set missile and aircraft velocities to zero to generate predictions of the static ground-test outcome. Predictions included the blast pressure profile, fragment spray pattern on the aircraft, fragment sizes, and fragment velocities.

PLANNING, PROVISIONING, AND TEST EXECUTION

While the 96 TG prepared and coordinated the test plan, NAWC obtained missile and full-up F-16 test assets. Test preparations continued with missile fore and aft body acquisition/fabrication, missile test stand fabrication, and instrumentation setup (as shown in Figure 1). Instrumentation consisted of an array of thin fragment-time-of-arrival plates affixed to the aircraft's upper skin and redundant arrays of blast pressure gauges at varying radii from planned detonation center. Aircraft fuel tanks were filled with water. This action allowed projectile-induced hydrodynamic ram without risking fuel fire that might destroy the aircraft before damage could be assessed. After a few pretests to gather early data and verify suitability of the test setup, NAWC positioned the Test #1 missile above the aircraft exactly as modeled. Although the test was limited to an endgame assessment, missile-aircraft engagement circumstances remained combat representative. Test #2 went much the same. All data necessary for Endgame Manager validation were obtained.

POST-TEST ANALYSIS

Aircraft damage assessment began immediately after Tests #1 and #2. These assessments began by capturing dimensioned photographs and recording positions of all fragment penetrations. Damage assessment continued with high-resolution 3-D laser scans of the

entire aircraft surface. When contrasted with baseline 3-D scans, the locations and dimensions of every change to the aircraft surface were quantified, including every fragment hole, dent, and element of blast deformation.

As illustrated in Figure 2, the 3-D scans were then correlated with Endgame Manager damage predictions by projecting an orthogonal coordinate system on the F-16 scan. This correlation/project allowed definition of x,y,z coordinates for every point on the aircraft and the test setup (e.g., pressure transducer location) with a high degree of accuracy. Impact points predicted by Endgame Manager were translated into this aircraft scan coordinate system and then overlaid onto the scan data as a separate computer-aided design (CAD) layer. This action enabled qualitative and quantitative comparisons of the number of predicted vs. actual impacts in a given area. The 3-D scans also defined sensor locations and (with precisely known distances) ensured the accuracy of fragment velocity calculations for model validation.

Upon conclusion of testing, JCAT and the 388 AMXS arrived to assess the total extent of aircraft damage and estimate damage effects on aircraft operation. Damage assessments began with Test #1. Blast damage and each element of fragment damage were traced along their shotlines to determine damaged components. Components damaged by blast/fragmentation were noted by JCAT and functionally identified by the 388 AMXS. Findings were recorded directly on 3-D scans of the damaged aircraft to eliminate ambiguity. Once all damages were noted, the 388 AMXS considered Test #1 damage as a whole and rendered an estimate of how the overall damage state would affect aircraft operation had this been an actual combat incident. JCAT and the 388 AMXS performed a similar analysis for the stand-alone Test #2 damage state. Beyond Endgame Manager, results of this detailed damage analysis are being used to assess the credibility of fault trees within aircraft vulnerability assessment codes.

SUMMARY

Through joint-Service collaboration, warhead damage effects data were gathered for validation of Endgame Manager. Not only was care taken to allow direct correlation of tested and modeled engagement scenarios, but application of a high-resolution laser scanner ensured precision of all measurements critical to the project's success. These high-resolution scans also proved useful to the JCAT team for documenting damaged systems without ambiguity. Ultimately, scanned data provided a valuable, permanent, and quantifiable archive of each test event. In addition, should future analyses be required, or if questions arise about the test, scanned data can be revisited for additional measures.

At the end of the day, every possible engagement condition and TTP countermeasure and maneuver are graded via M&S. Endgame Manager makes the final determination of whether a TTP passes or fails. Validation of Endgame Manager, through data produced by this effort, provides greater confidence that

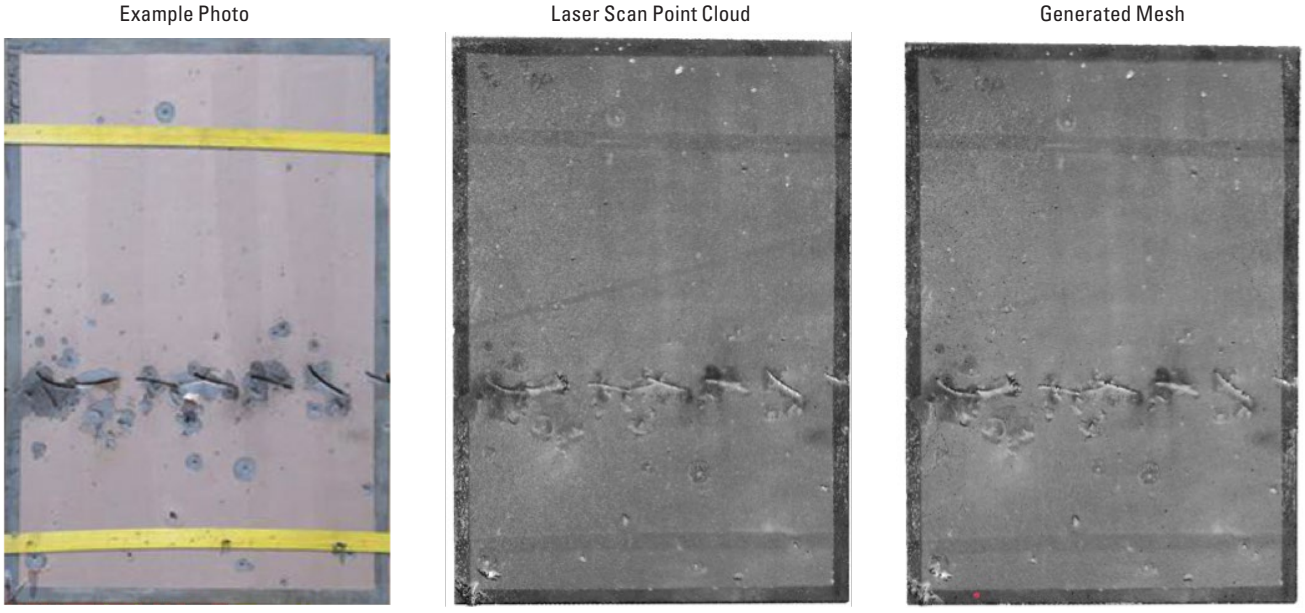

Figure 2 Photographed, Scanned, and CAD-Generated Damage for Analysis

TTP countermeasures are effective and that pilots called upon to employ them have the best odds of successfully accomplishing their mission and returning safely home to their families. May the odds be ever in their favor! ASJ

ABOUT THE AUTHORS

Mr. Greg Czarnecki is the Research, Development, Test, and Evaluation Team Lead for the 96 TG's Aerospace Survivability and Safety Office. For the past 35 years, he has supported aircraft survivability testing and modeling. Mr. Czarnecki holds an M.S. in materials engineering from the University of Dayton and is a member of JASP's subject-matter expert team for aircraft vulnerability reduction.

Mr. Ron Schiller is the Range Engineering Section Head for NAWCWD's Weapons Survivability Laboratory. He has supported survivability LFT&E efforts at China Lake for the past 20 years. Mr. Schiller holds a B.S. in mechanical engineering from California State University, Fresno, and an M.S. in mechanical engineering from California State University, Northridge.

Mr. Mitch Shedden is a vulnerability analysis engineer for the Combat Effectiveness and Vulnerability Analysis Branch, AFLCMC/EZJA. For the past 5 years, he has provided M&S subject-matter expertise in support of LFT&E for Acquisition Category I programs. Mr. Shedden holds a B.S. in mechanical engineering and an M.S. in materials science engineering from Ohio State University.

Mr. John Haas is the Vice President of Technical Services for Skyward, Ltd. His 25-year career in aircraft survivability/vulnerability testing and analysis has included ballistic live fire test and evaluations of numerous Air Force and Navy aircraft, as well as programs to assess threat weapon characterizations, evaluate materials, and evaluate vulnerability reduction concepts. Mr. Haas holds a B.S. in engineering physics from Ohio State University and an M.B.A. from Wright State University.

JCAT Corner continued from page 5

In addition, the team maintains both NIPR (*https://intellipedia.intelink.gov/wiki/ASDAT)* and SIPR (*https://www.usaace.army.smil.mil/asdat/info/asdatnewletter.htm)* websites to provide information on aviation survivability along with trending data from current operations. The biggest contributions to the portals are the weekly intelligence summary (INTSUM) and the quarterly newsletter, and both products can be found on the team's SIPR portal. The team works diligently to maintain its knowledge management efforts and anticipates more than 100,000 aviation survivability product downloads this year.

With the recent realignment to the requirements directorate (TCM-AB), Army JCAT has been finding new ways of helping the information flow from the warfighter to the requirement writers for the Army. Along with those efforts, the Aviation Shoot Down Assessment Team (ASDAT) has been working on the development of tactics, techniques, and procedures (TTPs) for future conflicts with technology-savvy adversaries. ASDAT has visited all the sister Services' tactics schools to collaborate and collect information on the development of these TTPs while sharing what is learned with each visit. This initiative will pay huge dividends for the survivability of our aircrews and help the aviation community as a whole.

Finally, Army JCAT has undergone some personnel changes this year. We are welcoming CW3 Chris Crawford, who comes from the TACOPS course at Fort Rucker, as well as CW3 Mike Clark, who recently joined us from the 82nd Combat Aviation Brigade. Both of these individuals have a wealth of knowledge and experience from multiple deployments downrange and are eager to help the JCAT program. We are also saying farewell to the current ASDAT Chief, CW5 Mike "el Jefe" Apple, who has been selected and assigned to the U.S. Army Forces Command (FORSCOM) G-3 Aviation Resources Management Survey (ARMS) team at Fort Bragg, NC. The team appreciates his tireless efforts and wishes him and his wife blessings on their next adventure. At the same time, the team welcomes his replacement, CW5 Scott Brusuelas, who comes from the 101st Combat Aviation Brigade (CAB) at Fort Campbell, KY, where he served as the brigade Tactical Operations (TACOPS) officer. He also has spent time flying OH-58Ds and UH-60Ms on multiple deployments. ASJ

EFFICIENT FLARE COUNTERMEASURES AGAINST INFRARED GUIDED THREATS

By Yeondeog Koo, Unseob Jeong, and Wonseok Choe

U.S. Air Force Photo

Portable infrared (IR) guided missiles have been the biggest threat to aircraft, especially low-speed helicopters, for the last several decades. The development of IR-based seekers for missile guidance has been an especially active research field, resulting in various emerging and/or advanced technologies, such as spin scan, conical scan, Rosetta scan, and image seekers [1]. Likewise, numerous aircraft countermeasures (CMs) against these threats, including flares, infrared countermeasures (IRCM), and directed infrared countermeasures (DIRCM), have been developed. And as aircraft have had countermeasuring equipment installed, the seekers have adopted infrared counter-countermeasures (IRCCM).

There are currently three major IRCCM capabilities: intensity rise time, line-of-sight (LOS) rate change, and spectral distribution discrimination [1–5].

- **Intensity Rise Time** - Although an aircraft has constant IR intensities, flares have abruptly increasing intensities right after burning. This increase is to get sufficient intensities before separating from the aircraft. Accordingly, a missile seeker has an intensity rise time trigger, enabling the seeker to recognize a flare when its intensity increases abruptly and discontinue tracking it.

- **LOS Rate Change** - IRCCM seekers can distinguish an aircraft-fired flare as a decoy by measuring the angular velocity of two objects when a flare separates rapidly from the aircraft right after firing. Thus, to delude the seeker, the aircraft must operate and launch flares in an effective manner.

- **Spectral Distribution Discrimination** - Seekers have IRCCM to detect flares by comparing the intensity ratios of an aircraft and flares in the near- and mid-IR regions. An aircraft has relatively constant intensities in the two IR regions, but flares have high

intensities in the near IR. Therefore, flares have been developed recently to increase the intensities in the mid-IR region, providing similar ratios to an aircraft.

This following sections discuss effective flare operation methods against LOS rate change of IRCCM. First, we introduce the experimental approaches that were conducted to characterize flight features of flares and an aircraft regarding the LOS rate change of IR seekers. The first set of experiments, flare firing, was performed to acquire trajectory and speed characteristics of flares with different conditions. The focus of the second set of experiments was on LOS rate change measurement using an actual IR seeker. Based on the analysis of these experiments and their resulting data, several flare firing management approaches are suggested to maximize aircraft survivability.

EXPERIMENTS

Flare Firing Experiments

For this study, flare trajectories from an actual firing test were studied, while previous studies have relied on simulation data [3, 6]. In the case of the simulation, the model was designed such that the flare weight and velocity decrease as the simulation time elapses, while the acceleration value reaches its maximum at burn-out time. For this study, the actual flare range, speed, and acceleration were obtained by the firing test.

In the experiment, conventional-type flares were fired to the horizontal direction from a hovering helicopter, and video was taken in the direction perpendicular to the flare motion direction. Based on this video, the effective time of the flare was measured to be approximately 4 s. The video was subdivided into 0.1-s intervals, and the distance was measured horizontally and vertically using some reference value of helicopter specifications for 4 s. The trajectory is shown in Figure 1, with just flare movements and no helicopter velocity elements. The trajectory equations were approximated by using polynomial interpolation. The horizontal and vertical speeds are shown in Figure 2, where the initial speed is 50 m/s and the final horizontal speed is almost 0.

Relative Speeds of Helicopter and Flares Viewed From the Missile

Assuming the helicopter speed to be 120 nm (60 m/s), the relative speeds of the helicopter and the flares viewed from the incoming missile were analyzed for 4 s, with the flare firing angle varying from 0 to 150° (see Figures 3–5). The angles of the incoming missile were also supposed to be from 0 to 150°. In the analysis, the flare speeds obtained in the experiments were applied, being attenuated for 4 s.

In the figures, the relative speed of the helicopter and flares can be seen to decrease as flares are fired in the direction similar to the helicopter movement, regardless of missile viewing angles. The speed is approximately 30 m/s, which is 50% of the helicopter speed (60 m/s), except when firing backward. The maximum values are similar to helicopter speed (60 m/s). The relative horizontal positions of the two were measured for 4 s in different firing angles (see Figure 6). The vertical values are changed to 40 m for 4 s in Figure 1.

The values in Figure 6 were used to measure the length of time that the target and flares simultaneously stay in the field of view (FOV) of a missile, assuming 2° (see Table 1). The longer the time in the FOV, the better the decoying. One reason is that the smaller the separation rate of the flares and target, which is LOS rate change, the better it is against the IRCCM seeker. Another reason is that the seeker cannot track a target normally when seeing the target and the flares simultaneously. Table 1 shows the longer time length as the flare firing angle gets closer to the helicopter heading direction.

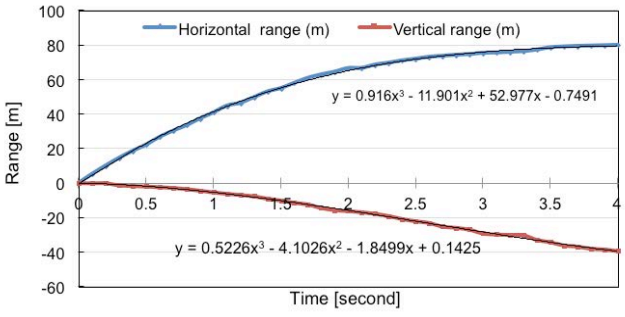

Figure 1 Flare Trajectories (Horizontal and Vertical Ranges)

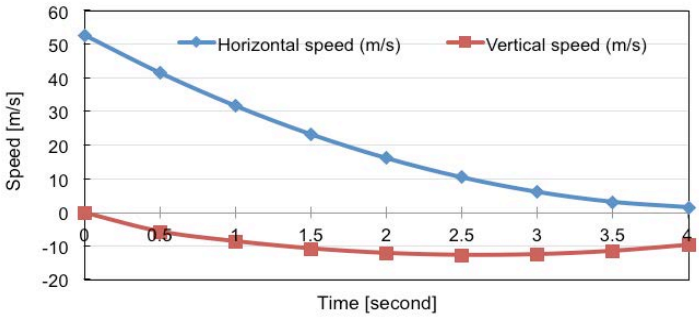

Figure 2 Relative Speeds (Incoming Missile Angle: 30°)

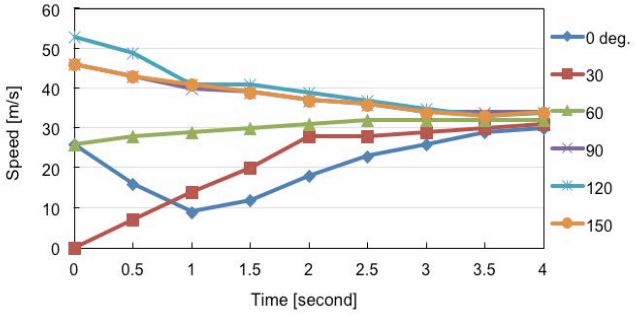

Figure 3 Relative Speeds (Incoming Missile Angle: 30°)

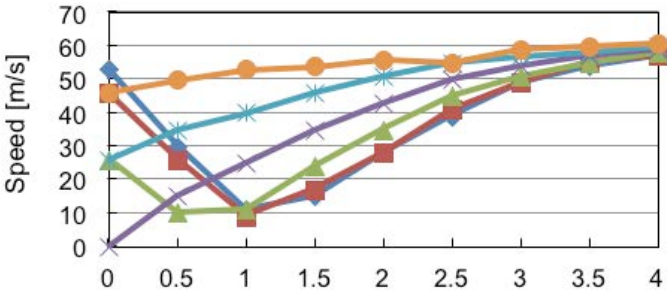

Figure 4 Relative Speeds (Incoming Missile Angle: 90°)

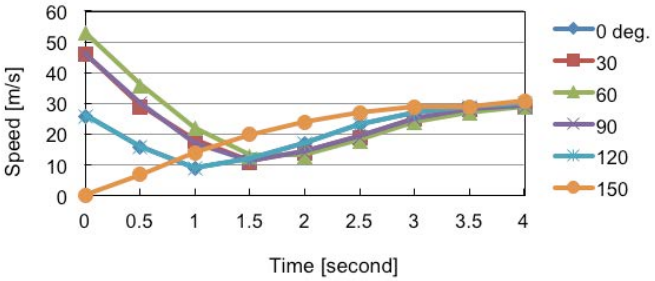

Figure 5 Relative Speeds (Incoming Missile Angle: 150°)

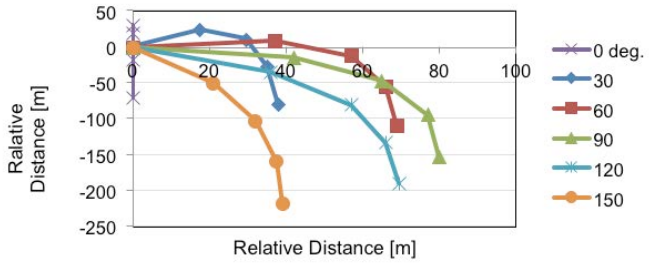

Figure 6 Relative Horizontal Positions of Helicopters and Flare for 4 s

LOS Rate Change Experiment

The trajectory sensing performance and LOS rate change function of an IR missile were tested in the laboratory (the setup of which is shown in Figure 7). The seeker used in the experiment was one of the units under test. Two IR sources were located 10 m from the seeker and heated to 2,000 °C. The heat sources areas, which were assumed to be a helicopter and flare, were changed to control IR intensities. It is generally known that flare IR intensities are 2–10 times greater than helicopter intensities in near IR [1]. In some experiments, the intensities were reported to be 50–100 times greater. In this study, the IR intensities of the flare varied between 10 and 110 times greater than the intensities of the helicopter.

The helicopter IR source, which has a weak intensity, was fixed in a location, and the flare source was moved along the tangential direction of the seeker with different speeds and intensity. The seeker was checked to determine whether to track the strong IR source, the flare. The maximum speed at which the tracker could keep tracking the weak source was recorded at different flare intensities. In the experiment, the angular velocities were increased according to two intensities ratios. The measured angular velocities and LOS rate changes are shown in Figure 8.

ANALYSIS

In studying the trajectories of flares fired from a helicopter, the separation speed viewed from an incoming missile was found to be approximately 30 m/s, which is half of the helicopter speed (except when fired in backward directions). The actual LOS rate change tested in the laboratory was betweem 2.3 and 6.3°/s. By applying these two values mathematically, we can conclude the flare decoy distance is 270–750 m from the helicopter. Thus, the flare can delude an incoming missile if the missile is further than this distance from the aircraft.

In a high-speed aircraft, the flare firing speed is relatively small compared to the aircraft. Therefore, the separation speed of the two will be the same as the aircraft speed regardless of firing angles. Assuming the aircraft speed to be 300 m/s, the flare decoy distance is 10 times that of a helicopter. Therefore, considering the missile effective range (3,000–5,000 m), it is nearly impossible to delude the missile by flare. To increase the survivability of high-speed aircrafts, installing flares with improved aerodynamic characteristics could be considered to minimize air resistance and increase flare speed near to the aircraft speed. These effects can increase the effectiveness by decreasing the separation speed [5, 7].

Table 1 Length of Time Staying in the FOV of Missile (Target and Flare Simultaneously)

Range	FOV	30°	60°	90°
1,000 m	35 m	2.5–2.7 s	0.9–2.3 s	0.8–2.2 s
2,000 m	70 m	3.5–4 s	2.5–4 s	1.7–3.2 s
3,000 m	105 m	4 s	3.5–4 s	2.6–4 s
4,000 m	140 m	4 s	4 s	3.3–4 s

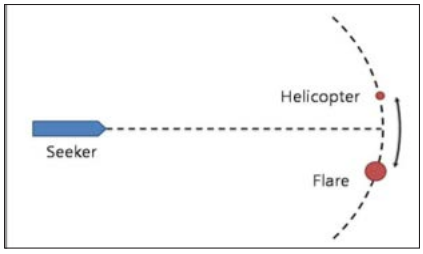

Figure 7 Experimental Setup

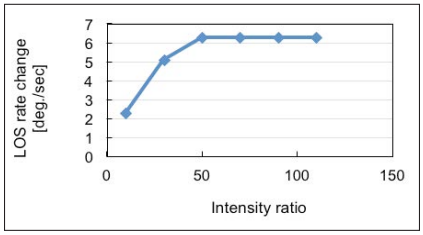

Figure 8 Measured LOS Rate Change

The ultimate measure to protect an aircraft against IR missiles is to fire flares several times repeatedly. IR seekers, seeing flare appearance, operate in three steps: flare detection, CCM tracking, and normal tracking [1–3]. If a flare is fired again before the seeker transits back to the normal tracking mode (in the case of exceeding the LOS rate change), it is considered possible to delude the seeker. The time interval is predicted to be related to the signal process period of the seeker, which is a unique specification for each seeker. Considering the aircraft-speed-calibrated flight trajectory of flares [6], two flares per 0.1 s will be able to mask the aircraft detection by the LOS rate change function.

The number of times the two rounds of flares with a 0.1-s firing interval are suitable and the amount of time interval that is needed are related with the missile flight time and effective flare time. Flares should be effective during missile flight. For example, if we assume the missile flight time to be 6 s, two rounds of flares with a 0.1-s interval should be fired and repeated two times more with a 1-s interval between repetitions.

Generally, passive missile warning sensors are widely used because of their covertness, but they also have the disadvantage of not knowing the missile distance and arrival time. Adding active sensors can control the numbers of flares firing because the arrival time is known. This addition/control will increase the effectiveness and also reduce false alarms.

CONCLUSION

Based on the experimental results from obtaining the relative flare speeds separated from a helicopter under various conditions and measuring the LOS rate change function, the following conclusions regarding effective flare firing techniques are made. For low-speed aircraft, such as helicopters, firing one round of flare can be effective against LOS rate change-based IRCCM seekers. With aircraft operational factors, such as safety, not considered, firing in the forward direction showed better results than firing in the backward direction. In the case of high-speed aircraft, IRCCM seekers can easily differentiate flares from aircraft due to high LOS rate change. Installing aerodynamically designed flares can help reduce the detection probability. Finally, for both low- and high-speed aircraft, firing two rounds of flares with a 0.1-s interval and repeating the firing several times is considered to be highly effective. ASJ

ABOUT THE AUTHORS

Dr. Yeondeog Koo works for the Agency for Defense Development in South Korea. He was the project manager for the Mission Equipment Package research and development (R&D), including Aircraft Survivability Equipment (ASE) for helicopters, and he is experienced in R&D and the test and evaluation (T&E) of various ASE, including the computer, missile warning system, radar warning system, laser warning system, and chaffs and flares.

Dr. Unseob Jeong is currently the team leader for the Agency for Defense Development's Electronic Warfare Systems and is a former project manager for the ASE system R&D for helicopters.

Mr. Wonseok Choe manages and develops the Electronic Warfare Experiment Laboratory for the Agency for Defense Development.

References

[1] Deyerle, M. "Advanced Infrared Missile Counter-Countermeasures." *Journal of Electronic Defense*, January 1994.

[2] Viau, C. R. "Implementation of Intensity Ratio Change and Line-of-Sight Rate Change Algorithms for Imaging Infrared Trackers." *Infrared Imaging Systems: Design, Analysis, Modeling, and Testing XXIII, Proceedings of SPIE*, vol. 8355, 2012.

[3] Forrai, David P., and James J. Maier. "Generic Models in the Advanced IRCM Assessment Model," P*roceedings of the 2001 Winter Simulation Conference*, 2001.

[4] Viau, C. R. "Expendable Countermeasure Effectiveness Against Imaging Infrared Guided Threats." Second International Conference on Electronic Warfare, Bangalore, India, 2012.

[5] Koch, Ernst-Christian. "Pyrotechnic Countermeasures: II. Advanced Aerial Infrared Countermeasures." *Propellants, Explosives, Pyrotechnics*, vol. 31, no.1, 2006.

[6] Baqar, S. "Low-Cost PC-Based High Fidelity Infrared Signature Modeling and Simulation." Ph.D. thesis, Cranfield Defense and Security, 2007.

[7] Labonte, Gilles, and W. C. Deck. "Infrared Target-Flare Discrimination Using a ZISC Hardware Neural Network." Jo*urnal of Real-Time Image Processing*, 2010.

YOUNG ENGINEER IN SURVIVABILITY
JAMIE EDWARDS

by Linda Moss

The Joint Aircraft Survivability Program Office (JASPO) is pleased to recognize Mr. James (Jamie) Edwards as its latest Young Engineer in Survivability. An accomplished operations research analyst, Jamie works in the Survivability/Lethality Analysis Directorate (SLAD) of the U.S. Army Research Laboratory (ARL) at Aberdeen Proving Ground, MD.

His career in survivability began in 2003, when he was a high school student contractor at ARL, and he continued to work part time at the laboratory throughout his college years. During that period, he collaborated with senior scientists and engineers to develop and employ computer models and simulations for assessing the vulnerability of Army combat systems, both ground and air, to conventional threats.

In 2008, after graduating from the University of Maryland with a double major in mathematics and economics, Jamie transitioned to full-time employment in SLAD's System Engineering and Experimentation Branch (SEEB). Since then, he has worked on projects managed by the major tri-Service survivability/vulnerability (S/V) programs (e.g., JASP and Joint Live Fire [JLF]) as well as performed S/V and lethality research in ARL/SLAD core mission areas. Now, with 13 years of combined empirical and analytical experience in S/V, Jamie is a technical project leader in SEEB. His most recent assignments include conducting live-fire testing to refine analytical methods for predicting shock-induced detonation of warhead explosive materials. This predictive capability is an important factor for determining lethality in a Live Fire Test & Evaluation (LFT&E) program for a major Army air-defense missile system.

The following sections describe some of Jamie's accomplishments in S/V, reflecting his technical abilities, work experience, and professional involvements.

FUEL SYSTEM VULNERABILITY

Jamie was introduced to the vulnerability of fuel systems when assigned to a JASP project to determine ballistic limits, hole sizes, and leak rates for self-sealing bladder materials by testing. For that work, he became proficient with the FATEPEN and ProjPen models, and his understanding of the predictive influences of the models' inputs was instrumental in ensuring that the appropriate parameters were measured in those tests.

Jamie is also an acknowledged expert on the Fire Prediction Model (FPM). He has performed sensitivity studies on the effects of varying FPM inputs (e.g., striking velocity, air gap distance, function type, and interior (target) geometry) on the model's estimates of fuel ignition and fire sustainment, and he has run FPM for target-specific vulnerability analyses, including ground systems. For example, he generated air gap tables used to assess fires on missile-launcher and jammer systems for the Joint Technical Coordinating Group for Munitions Effectiveness (JTCG/ME) and the High Mobility Multipurpose Wheeled Vehicle (HMMWV) for an Army studies program. He is also responsible for pre-shot predictions with FPM, most recently for the JASP-sponsored fuel subsystem ullage vulnerability test on the tri-Service C-12 airplane.

In addition, Jamie led the JASP-sponsored FPM Ignite verification and validation (V&V) program, partnering with Air Force, Navy, and industry (SURVICE Engineering Company) representatives to identify and fix discrepancies between the source code and documentation, fix implementation errors, and validate the model via simulation. He also serves as the Army representative for the FPM Configuration Control Board and is currently involved in planning efforts for the Next-Generation Fire Model.

Jamie also developed inputs to the JASP and JTCG Joint Data Repository. This database allows for a unified collection of impact flash and hydrodynamic ram parameters, as well as types of incendiary functions by projectiles, to help standardize test and measurement practices. Reports and data contained in this repository are available for model development and validation.

PERSONAL PROTECTIVE EQUIPMENT (PPE)

In the area of PPE, Jamie has conducted tests and performed analyses on multiple programs for the Warfighter, including a comprehensive statistical assessment of selected hard body-armor plate designs for the Project Manager for Soldier Protection and Individual Equipment (PM-SPIE) and the Director of Operational Test and Evaluation (DOT&E). Rigorous ballistic testing was conducted to characterize ballistic performance and to show with high confidence the probability of no perforation along with the upper tolerance limit of the back-face deformation. Performing logistic regression using general linear models/maximum likelihood estimation, Jamie developed the response curves of the probability of perforation as a function of striking velocity and computed the parameter estimates of the response curves and the associated standard deviations to obtain confidence intervals on the ballistic limits. This assessment helped lead DOT&E to establish standard body-armor test procedures and criteria.

Jamie was also instrumental on several PPE programs, including characterizing the ballistic performance of the Improved Outer Tactical Vest (IOTV) collar and research studies to (1) evaluate different free-air mounting methods for testing soft body armor and (2) determine whether the phenomenon called shatter gap occurred when testing certain bullets against hard body-armor plates.

MATERIAL CHARACTERIZATION

Jamie implemented this response curve methodology for material characterization of the target-threat interactions to improve the modeling capability of ProjPen. He developed the test plans, led range personnel on ballistic testing, and conducted analyses to get the required data to update the tri-Service penetration equations. Along the way, he also developed a mathematical method for obtaining unbiased measurement of residual velocity during ballistic testing when only a single high-speed camera is available.

CARGO ON/OFF LOADING SYSTEM (COOLS) ARMOR

Jamie led the statistical analysis for the Army's CH-47F Chinook LFT&E program to determine the ability of the aircraft's ballistic protection system (BPS)—integrated with the COOLS flooring—to shield against small-arms threats. BPS and COOLS are product improvements new to the CH-47F. From the ballistic testing, Jamie computed ballistic limit parameter estimates of the response curves that provide the probabilities of armor penetration as a function of striking speed and obliquity. These functions are the underpinning of the CH-47F force-protection analysis (i.e., the level of ballistic protection afforded to the aircrew and passengers by the helicopter) and produced major improvements in vulnerability assessment resolution and accuracy. ASJ

MISCELLANEOUS

Outside of work, Jamie is pursuing a master's degree in applied mathematics at Towson University. In addition, since 2011, he has served in several capacities for the Chesapeake Chapter of the American Statistical Association, including membership chair, newsletter editor, vice president, and, currently, president. He is also an accomplished guitar player for the local band The Rivals. He also enjoys spending time in the mountains of western Maryland with his wife, Tara.

ABOUT THE AUTHOR

Ms. Linda Moss is the Statistics Team Leader in the System Engineering and Experimentation Branch of ARL/SLAD. She has more than 30 years in ballistic testing, methodology, and analyses of ground and air systems for both survivability and lethality programs. Currently, she serves on the JASP Vulnerability Assessment and Reduction committee. Ms. Moss holds B.S. and M.S. degrees in statistics from Virginia Tech and the University of Delaware, respectively.

FINDING OIL-LOSS SOLUTIONS FOR ROTORCRAFT DRIVES

by Stephen Berkebile, Jason Fetty, Robert F. Handschuh, and Brian Dykas

A helicopter's drive system converts the high rotational speed from engine output shafting into the lower rotational speed and higher torque required by the main and tail rotors for flight, with accompanying changes in shafting orientation. Transmission gearboxes within the drive system contain gears and bearings that are subjected to punishing loads and contact stresses as they transmit several thousand horsepower. Proper supply of oil within the gearboxes is critical to the continuing function of the drive system under these strenuous internal conditions during flight. If this lubricant supply is compromised, degradation in the drives will rapidly lead to loss of power and a forced landing, or worse.

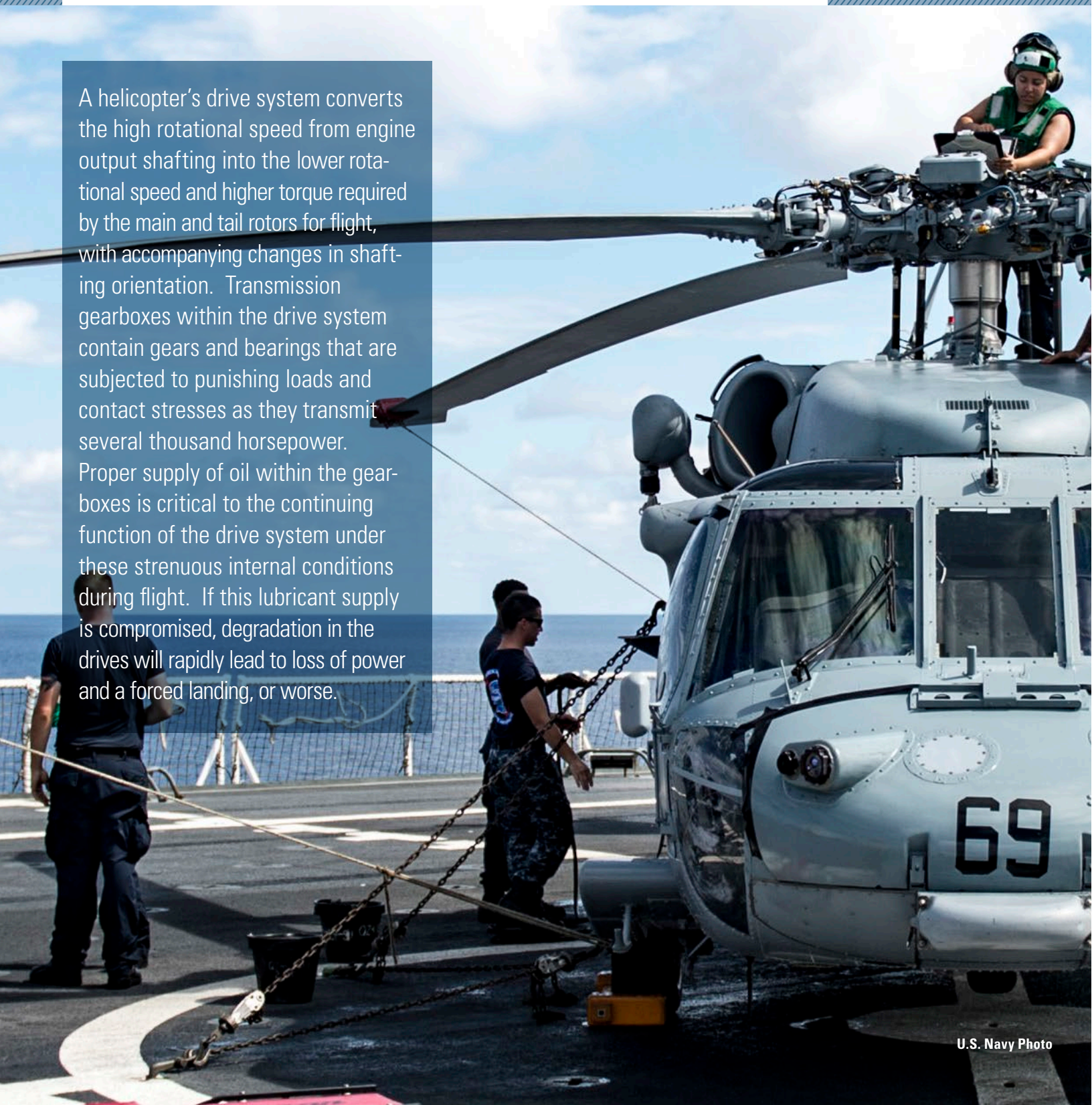

U.S. Navy Photo

THE PROBLEM OF PROPER LUBRICATION

Oil in a power transmission or gear box serves multiple purposes. The primary roles are lubrication of contacting surfaces and temperature regulation by removal of heat. Under normal operating conditions, an extremely thin film of oil separates gear and bearing surfaces, preventing direct metal-to-metal contact, reducing friction, and allowing the components to operate through billions of cycles. Unfortunately, even with the reduced friction, contact between highly loaded components at high speeds in the gearbox causes substantial heat generation. One way to dissipate this heat, however, is through advection by the gearbox oil. Under normal rotorcraft operations, this gearbox oil is recirculated and cooled to keep heat generation low and remove excess heat.

An oil-out condition occurs when the primary oil flow to a gearbox is interrupted. This condition may result from a ballistic impact or any other event that blocks, impedes, or removes the oil supply to transmission components. Loss of the primary oil flow can result in an immediate or rapid failure of the drive system due to the reduced heat dissipation, increased friction (resulting in additional heat generation), and material degradation in the highly loaded gear and bearing contacts. Thermal growth in components leads to a decrease in gear backlash, which eventually causes binding and thermal runaway of these components. Seized gears can prevent the rotors from turning, so autorotation to a safe landing is not always possible in the event of loss of lubrication.

These events affect not just military aircraft, but civil aircraft as well. Recent transmission oil-loss incidents have caused emergency landings and fatalities. These incidents include a 2008 Sikorsky S-92 incident in which a transmission oil loss caused a forced emergency landing, a 2009 Sikorsky S-92 incident in which a transmission oil-loss event caused an aircraft crash and resulted in 17 fatalities, and a 2012 Eurocopter EC 225 incident in which a lubrication system failure caused a forced emergency landing [1, 2].

LOSS-OF-LUBRICATION PERFORMANCE

Army rotorcraft drive systems are subject to loss-of-lubrication design certification requirements, as described in ADS-50-PRF, which states that the drive systems are required to operate after loss of primary oil flow for a minimum of 30 minutes at cruise conditions (approximately 50% power rating) [3]. However, the Army desires the ability to run for a longer period of time after a loss-of-lubrication condition. Future platforms are planned to have longer endurance and range capabilities, requiring corresponding improvement in loss-of-lubrication performance to enable long-distance exit from hostile areas, ideally exceeding half-mission range.

The certification requirements of modern rotorcraft have resulted in oil-out performance of transmissions receiving considerable attention, and the rotorcraft community has increased scrutiny of this survivability aspect over the past few years as a result of the high-profile mishaps. Accordingly, government and industry organizations have increased research and development in transmission oil-out behavior.

Improving the oil-out survivability of the existing fleet is a great challenge, since modifying the gearbox and constructing new drop-in gearboxes both require extensive flight certification beyond the design and prototyping, and with no guarantee that the requirement will be achieved. In some cases, the 30-minute requirement has been met by the addition of secondary emergency lubrication systems external to the gearbox. However, secondary systems add complexity and weight to the vehicle, especially if they contain their own lubricant supply, and thus they are not always feasible.

Progress has recently been made in the design of a new transmission, with the Augusta-Westland AW189 main gear box lasting more than 50 minutes during its certification [4]. Augusta-Westland's holistic approach in combining materials and design elements demonstrates that improvement is possible with a new design. Nonetheless, developing solutions that can be applied to new and existing systems with little or no internal modification would also be desirable.

PAST AND CURRENT EFFORTS

Over the last 15 years, loss-of-lubrication research has been conducted at NASA Glenn Research Center on a test facility originally intended to conduct surface contact fatigue experiments on gears (see Figure 1). NASA's initial work in this area produced some inconsistent results [5], so a larger test series was conducted that concentrated on making the test section of the gearbox more like that of a high-speed, aerospace gearbox [6]. During this series of approximately 60 tests, many configurations were assessed, including

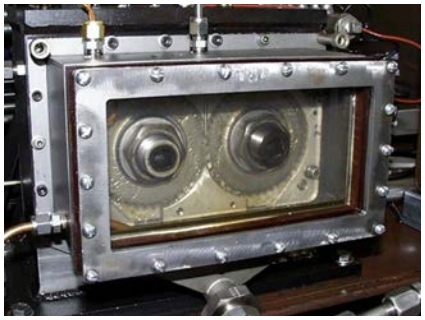

Figure 1 High-Speed Spur Gear Rig for Component-Level Evaluation

materials, shrouding, and gear designs. This work resulted in establishment of a loss-of-lubrication test procedure and rig configuration with considerably better repeatability during testing in terms of time-to-failure and facility temperatures recorded.

Once the test procedure and facility setup were established, enhanced testing was initiated, including determining the temperatures of the gear teeth during operation. In one study, gears were instrumented with thermocouples connected via slip rings to have on-component data during normal and loss-of-lube conditions, which has been useful in understanding gear bulk temperatures as compared to the static temperature measurements made in the gear shrouding. A recent development has been the addition of high-speed infrared imaging system to measure full-field temperatures of the gears while in operation (10,000 RPM) [7]. An example of the infrared temperature measurement of the spur gears during operation is shown in Figure 2. The temperature of the gear teeth is critical during failure, as can be seen in the glowing of gears seconds before failure in Figure 3.

Current and future work by the U.S. Army Research Laboratory and NASA combines approaches from both macroscopic and microscopic viewpoints and includes experimental work as well as efforts in modeling and simulation. One of the key unknown parameters is the heat generation while in oil-out conditions. Work directed toward a better understanding of how this parameter impacts loss-of-lubrication performance is needed to advance and improve loss-of-lubrication behavior. Penn State University has developed a multiphysics simulation that couples computational fluid dynamics and tribology (the study of friction and wear) modelling using heat generated [8]. This Army-supported project continues to advance the fidelity of the simulation.

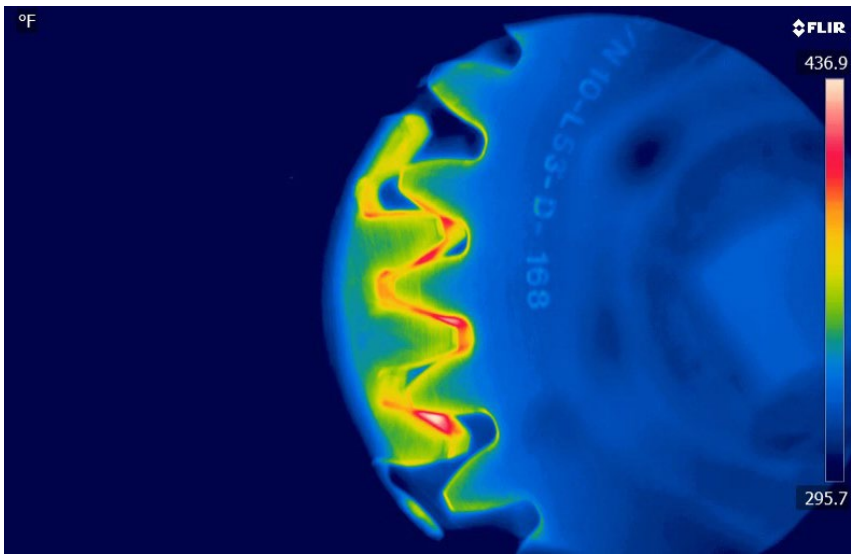

Figure 2 Spur Gear Temperature During Loss of Lubrication Measured by IR Emission

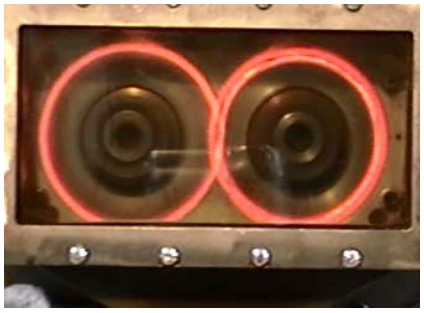

Figure 3 Spur Gears Operating After Oil Shutoff Glowing From Frictional Heating Shortly Before Failure

Another unknown is the detailed progression of microscopic material degradation during failure. Insight into these chemical and physical mechanisms will inform materials selection in the future.

As a part of these efforts, a current Joint Aircraft Survivability Program (JASP) project seeks to establish and rapidly transition an improved portfolio of technologies to increase transmission performance after the loss of the primary lubrication system, with the ultimate goal of increasing vehicle survivability and extending this period to at least half-mission duration. Many concepts to reduce heat generation, increase heat rejection, increase material tolerance to higher temperatures, and increase material resistance to damage have been considered and assessed over the past 2 years. This collaboration between the U.S. Army, U.S. Navy, and NASA was created to accelerate the work under way among various government and industry organizations and to join broad expertise and laboratory resources in a more unified, joint effort. The overall objectives are to:

- Identify and screen promising candidate technologies falling within the realm of lubricant science and tribological surfaces.

- Determine the effectiveness of screened technologies at the component level in spur gear testing.
- Perform a full-scale loss-of-lubrication experiment on an H-60 transmission, incorporating screened technologies as appropriate, to demonstrate improved performance when compared to a baseline.
- Record data from a suite of instrumentation to provide critical data that will be useful for verification and validation of emerging multiphysics simulation tools.

Choosing technologies to implement requires consideration of several factors, such as cost, ease of implementation, and compatibility between the technologies. Although operating the flight-qualified full transmission allows freedom to include system-level and mature approaches, the intent is to develop cutting-edge enabling technologies with potential for implementation in multiple platforms within a 3- to 5-yr time period. With this goal in mind, the technologies selected for final implementation are intended to be widely applicable across platforms, even if those technologies will require further qualification and optimization efforts before use in a vehicle.

FINDING LOSS-OF-LUBE TECHNOLOGIES

The approach that we have taken to identify and develop promising loss-of-lubrication technologies is designed to rapidly move those technologies along the Technology Readiness Level (TRL) path. The approach begins with screening emerging technologies using coupon-level methods. Then those showing promise are implemented at the component level, followed by a final selection and simultaneous evaluation of a suite of technologies at the system level. In this way, the tradeoffs between simpler and inexpensive coupon evaluation can be balanced with the greater fidelity of the more complex and costly gear evaluation. The approach is nevertheless ambitious considering the desired schedule and distributed scope.

The coupon-level evaluation is conducted at the U.S. Army Research Laboratory on a high-speed tribometer, an instrument that allows for precise control over contact conditions between two objects (such as the ball and disc shown in Figure 4). The ball-and-disc tribometer can be used to simulate specific gear or bearing conditions and make a rapid determination of experimental parameters, such as lubricant properties, alloy properties, or the smoothness of the surface finish, as demonstrated in Figure 5. When the lubricant supply is stopped, one can extract a time-to-failure, as shown in Figure 6.

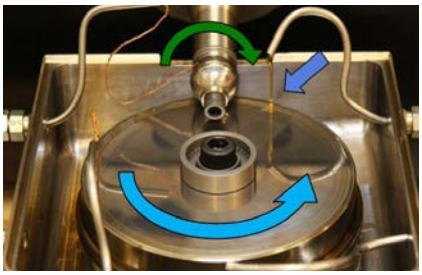

Figure 4 Coupon-Level Evaluation of Technologies With a Ball-on-Disc Tribometer

Figure 5 Coupons Demonstrating Different Surface Finishing Technologies

The component-level evaluation occurs on the spur gear rig at NASA Glenn Research Center, shown in Figure 1. The results of operation without oil can be seen in the glow of the gear teeth caused by frictional heating in Figure 3 and in the gears after failure shown in Figure 7. During these evaluations, we have taken care to ensure the conditions during coupon-level screening match well to those of the spur gear rig, and, as a result, the agreement between the two methods has been good. We anticipate similar results in the full transmission test to be conducted at the Patuxent River Naval Air Station in 2017.

Thus far, we have selected an aerospace lubricant with a phosphonium ionic liquid additive, developed under a Small Business Innovation Research (SBIR) program, a method of mirror-finish polishing called superfinishing, and the integration of hybrid bearings (containing silicon nitride ceramic rollers and Cronidur 30 steel rings) as the most promising technologies for integration into the full transmission test that can realistically be implemented within the

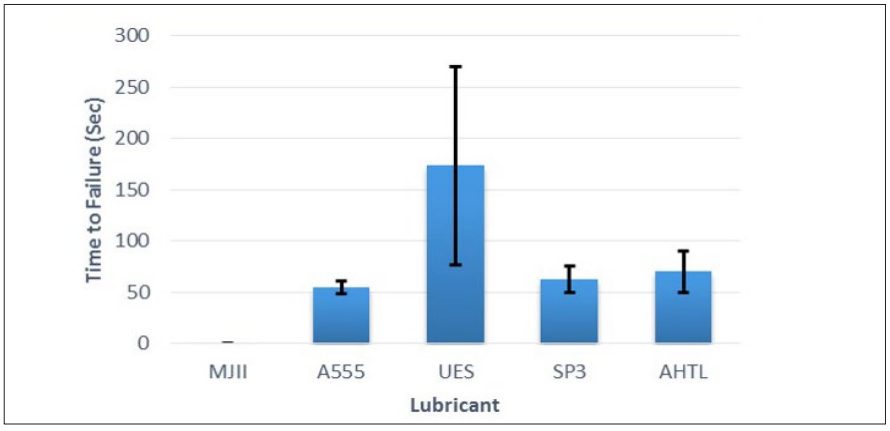

Figure 6 Time-to-Failure for Coupon Evaluation of Standard (MJII, A555) and Novel Lubricants (UES, SP3, AHTL)

Figure 7 Spur Gears After a Complete Loss-of-Lubrication Evaluation

scope of this project. Each of these technologies has demonstrated increased time-to-failure during our coupon- and component-level evaluation. The causes for why these technologies are providing an improvement in oil-out time are still being investigated.

Furthermore, work continues on identifying, understanding, and optimizing loss-of-lubrication technologies sponsored by parent organizations, and this list may evolve before final implementation in the full transmission. For example, gear coatings developed under another SBIR project are currently being investigated. Beyond the anticipated outcome of the full transmission test and the identification of several promising technologies (and determination of candidates that should not be used), much has been learned about the details of the physical processes during a loss-of-lubrication event. The data collected at all three levels (coupon, component, and system) will be used to direct the advance of models and simulations for design and in the identification of promising directions for future material and lubricant development.

ASJ

ACKNOWLEDGMENTS

The authors would like to acknowledge others who have made, and continue to make, significant contributions to the current JASP effort. These individuals include Radames Colon-Rivera, Kevin Radil, Mark Riggs, Nikhil Murthy, Kelsen LaBerge, Timothy Krantz, and Eric Hille.

ABOUT THE AUTHORS

Dr. Stephen Berkebile conducts research at the U.S. Army Research Laboratory in tribology and lubrication sciences. He currently leads several projects studying lubricants, coatings, and materials for loss of lubrication and increasing power density, as well as the basic chemical and physical processes at work in high-speed contacts between materials. Dr. Berkebile has a Ph.D. and an M.S. in physics from Karl-Franzens-Universität Graz/University of Graz and a B.A. in physics and German from Manchester College.

Mr. Jason Fetty is an aerospace engineer at the Aviation Development Directorate - Aviation Applied Technology Directorate. He has worked in research and development of drive system technologies for Army rotorcraft since 2001, including participating in several major 6.3 drive system efforts, as well as multiple efforts involving gearbox loss-of-lubrication performance. Mr. Fetty has a B.S. in mechanical engineering from Virginia Tech.

Dr. Robert F. Handschuh is the Chief of the Rotating and Drive Systems Branch at NASA Glenn Research Center and the former leader of the Drive Systems Team. He has more than 30 years of experience with NASA and Department of Defense rotorcraft drive system analysis and experimental methods conducting research in high-speed gearing including windage, loss-of-lubrication technology, and hybrid gearing. Dr. Handschuh has a Ph.D. in mechanical engineering from Case Western Reserve University and a M.Eng. in mechanical engineering from the University of Toledo.

Dr. Brian Dykas leads the research in propulsion drives at the U.S. Army Research Laboratory. He has more than 10 years of research experience in the tribology of propulsion mechanical components. Dr. Dykas holds a Ph.D. in mechanical engineering from Case Western Reserve University.

References

[1] SKYbrary. "Accident and Serious Incident Reports: Rotary." http://www.skybrary.aero/index.php/Accident_and_Serious_Incident_Reports:_Rotary, accessed 10 January 2016.

[2] Transportation Safety Board of Canada. "Aviation Investigation Report A09A0016." 12 March 2009.

[3] U.S. Army Aviation and Troop Command. "Aeronautical Design Standard: Rotorcraft Propulsion Performance and Qualification Requirements and Guidelines." ADS-50-PRF, 15 April 1996.

[4] Gasparini, G., N. Motta, A. Gabrielli, and D. Colombo. "Gearbox Loss of Lubrication Performance: Myth, Art or Science?" *European Rotorcraft Forum 2014*, Southampton, UK, 2014.

[5] Handschuh, R. F., and W. Morales. "Lubrication System Failure Baseline Testing on an Aerospace Quality Gear Mesh." NASA/TM-2000-209954 and ARL-TR-2214, NASA Glenn Research Center and U.S. Army Research Laboratory, 2000.

[6] Handschuh, R., J. Polly, and W. Morales. "Gear Mesh Loss-of-Lubrication Experiments and Analytical Simulation." NASA/TM-2011-217106, NASA Glenn Research Center, Cleveland, OH, 2011.

[7] Handschuh, R. F. "Thermal Behavior of Aerospace Spur Gears in Normal and Loss-of-Lubrication Conditions." *American Helicopter Society 71st Annual Forum*, Virginia Beach, VA, 2015.

[8] McIntyre, S., Q. Yu, R. Kunz, L. Chang, and R. Bill. "A Computational System Model for Gearbox Loss-of-Lubrication." *American Helicopter Society 70th Annual Forum*, Quebec, Canada, 2014.

[9] Handschuh, R., J. Polly, and W. Morales. "Gear Mesh Loss-of-Lubrication Experiments and Analytical Simulation." NASA/TM-2011-217106, NASA Glenn Research Center, Cleveland, OH, 2011.

MODELING AND SIMULATION OF HYDRODYNAMIC RAM FOR AIRCRAFT SURVIVABILITY

by Kangjie Yang, Young W. Kwon, Christopher Adams, and David Liu

Hydrodynamic Ram (HRAM) refers to the damage process due to high pressures generated when a kinetic-energy projectile penetrates a compartment or vessel containing a fluid [1]. The large internal fluid pressure acting on the walls of the fluid filled tank can result in severe structural damage. The study of HRAM effects on fuel tanks used on military aircraft is vital if the designs can withstand HRAM loads due to a hostile environment.

Many types of threats could result in HRAM damage to aircraft fuel tanks, including armor-piercing rounds from small arms fire or fragments from missile warhead detonations. Statistics from Operation Desert Storm indicated that 75% of aircraft losses were attributable to fuel system vulnerability, with HRAM being one of the primary kill mechanisms [2]. A ruptured aircraft fuel tank and its damaged surrounding structures would likely require a long downtime for depot-level maintenance, as opposed to quick patch repairs of the entry wall panel. In other words, HRAM damage results in lower aircraft availability and higher cost of recovery. In some cases, HRAM could also lead to catastrophic attrition of the aircraft due to the cascading effect of fuel tank failure [3]. To design structures to withstand the HRAM loads, or to develop the HRAM mitigation techniques for existing aircraft, it is necessary to first predict the pressures distribution inside the tank at the different phases of the HRAM phenomenon.

The goal for HRAM research is to develop ways to eliminate the extensive damage to the entry and exit walls of the fuel tank immediately after being

impacted by a projectile. The objective of the study described herein was to model and simulate HRAM using a finite element (FE) technique [4] to analyze the dynamic response of a tank structure and conduct parametric studies on factors affecting tank wall response during the initial phase of the HRAM event. The model will enable a better understanding of how various parameters affect the pressure waves generated in the fluid, as well as the dynamic response of the coupled structure. For the parametric studies conducted, the emphasis was mainly on the structural exit wall response, where critical components or main structural members of the aircraft are typically located in close proximity.

REVIEW OF HRAM

In most nonexploding projectile impacts, in which the projectile penetrates and then traverses through a fluid-filled tank, the HRAM phenomenon can be described in four distinct phases [2]:

- **Shock Phase:** the initial impact of the projectile into the entry wall of the fuel tank
- **Drag Phase:** the movement of the projectile through the fluid
- **Cavitation Phase:** the development of the cavity behind the projectile as it moves through the fluid and the subsequent cavity oscillation and collapse
- **Exit Phase:** the penetration of the projectile through the exit wall and tank (when there is sufficient energy remaining).

Each phase contributes to structural damage of the tank walls via a different mechanism, and the extent of damage depends on numerous factors, such as projectile shape and velocity, fluid level in the impacted tank, obliquity of impact, and the material of the fuel tank [5]. The high cost of performing experiments to understand HRAM phenomenon has led to extensive efforts in developing numerical techniques for computational simulation. Such efforts have been attempted for the past 30 years, with earlier efforts trying to simplify the phenomenon into a structural response problem, with boundary conditions representing the applied loads from the pressure field generated by ram effects. Subsequent efforts attempted to solve the nonlinear sets of hydrodynamic equations using numerical techniques by coupling the fluid and structure interaction.

MODELING PROCEDURES

The HRAM model consists of Lagrangian mesh for the tank and projectile and Eulerian mesh for the fluid inside the tank. The simulation of HRAM required an extremely fine Euler mesh and small sampling times to capture the propagation of shock waves in the fluid, thereby resulting in large files and long computational times. For a computational model simplification, a generic 200-mm x 200-mm x 200-mm cubic tank impacted by a 10-mm-diameter spherical projectile was developed. Subsequent parametric studies on the tank wall response and fluid pressures during the different phases of the HRAM event were presented with this simplified fluid-filled tank model. This simplified model is generally much smaller than a typical fuel tank in aircraft. However, regardless of the size and simplification, the present model shows all the important HRAM characteristics.

The projectile impacting at the center of the tank's entry wall was a 4-g, 10-mm-diameter, solid steel sphere. It was considered as a rigid material. One reason for selecting a projectile with a spherical surface was to prevent the tumbling of the projectile during the drag phase, which would have resulted in significant pressure fluctuations in the fluid causing erratic response to the coupled tank walls. The 200-mm^3 tank was discretized with 9,600 quadrilateral shell elements with four grid points, as shown in Figure 1. The element size was set to 5 mm and was assigned properties defined as an isotropic, elastic-plastic material (the properties of which are provided later).

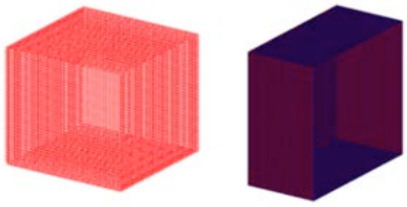

Figure 1 Lagragian Tank Model Consisting of 9,600 Shell Elements (left); Lagragian Tank Model cutaway (right)

The fluid in the tank was discretized with three-dimensional (3-D) solid eight-node hexahedron Eulerian elements. A total of 64,000 Eulerian elements made up the box with 5-mm element lengths. The fluid level and properties were varied for the different cases investigated. The mesh size for the Eulerian fluid elements was chosen to be similar to the Lagrangian tank shell elements, so the nodes are coincident to one another at the coupling surface. This condition is necessary for proper coupling of the Lagrangian and Eulerian elements to avoid unnecessary problems arising from the failure of the coupling surfaces.

As shown in Figure 2, two models were constructed for the purpose of this study. The first model (Model 1) was for the investigation of the shock phase of the HRAM, with the projectile outside the tank impacting the entry wall at a prescribed velocity. For this model, the

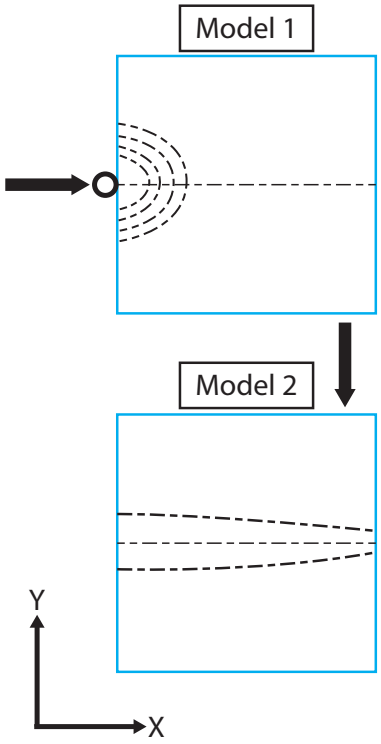

Figure 2 Model 1 and Model 2 Schematics

displacement of the tank walls due to projectile impact and the subsequent ram pressure of the propagating hemispherical shock wave in the fluid from the impact point are of interest.

For the second model (Model 2), the projectile initial starting position is flush to the inner surface of the entry wall at the impact point, simulating the projectile's position immediately after penetrating the entry wall. The initial velocity of the projectile is less than 250 m/s due to retardation of the projectile by the entry wall. Model 2 is used to study the fluid pressures and tank wall response during the drag phase.

The initial loads and boundary conditions for the two models are tabulated in Table 1. An important aspect of fluid structure interaction problem is the coupling of the surfaces between the structure and fluid mesh.

For Model 2, the projectile was coupled to the fluid by the general coupling technique while the fluid and tank surfaces were coupled together using the Arbitrary Lagrangian-Eulerian (ALE) coupling technique. In MSC Dytran, the general coupling mode allows the motion of a structure through a fixed Eulerian mesh, such as the movement of the projectile through the fluid. The Lagrangian structure, which is the projectile in this case, acts as a moving flow boundary for the fluid in the Eulerian domain while the fluid in turn acts as a pressure load boundary on the projectile.

For the ALE coupling technique used to define the interaction between the tank and fluid, the Eulerian mesh is now allowed to move and follow the motion of the Lagrangian mesh at the interface, since the nodes between the two meshes are now physically coupled together. When the tank walls start to displace, the fluid Euler mesh also moves together. Due to the motion of the Euler mesh, a compressive force is exerted on the adjacent fluid element. The compressed fluid element in turn exerts a pressure load back on the structural tank wall elements [6].

Tracer elements were defined at various locations within the model to collect data required for time-history plots of the tank wall displacement, velocity and stresses, and the fluid pressures for analysis. Locations of the tracer elements are illustrated in Figure 3. There were nine tank shell elements across the entry, left, and exit walls, and there were three fluid hex element tracers.

For ease of comparison and analysis, the graphs plotted were obtained from the middle node and element of each wall, labeled No. 1, 5, and 7 for the tank structure and Fluid 2 for the fluid pressures output. The material properties and constitutive models for baseline Model 1 and 2 are summarized in Table 2.

RESULTS AND DISCUSSION

Even though a typical HRAM event consists of four phases, it was decided this study would analyze the impact phase separately using Model 1, as the failure process of projectile penetration and the subsequent material failure are still not well modeled at present. To avoid the unclear nature and the possible ambiguity in the results, it was determined that the modeling of projectile penetration into and out of the tank be omitted from the simulation. Data collected to plot the time history for the tank wall's displacement,

Table 1 Loads and Boundary Conditions

Loads and Boundary Conditions	Description
Displacement	Model 1: Bottom surface of tank is fixed Model 2: Bottom surface of tank is fixed
Projectile Initial Velocity	Model 1: 300 m/s Model 2: 250 m/s
Contact	Model 1: Master-slave surface contact between projectile and tank Model 2: Adaptive master-slave contact between projectile and tank
Coupling (between fluid and projectile)	Model 1: Nil Model 2: General coupling
Coupling (between fluid and tank)	Model 1: Arbitrary Lagrangian-Eulerian (ALE) coupling Model 2: ALE coupling

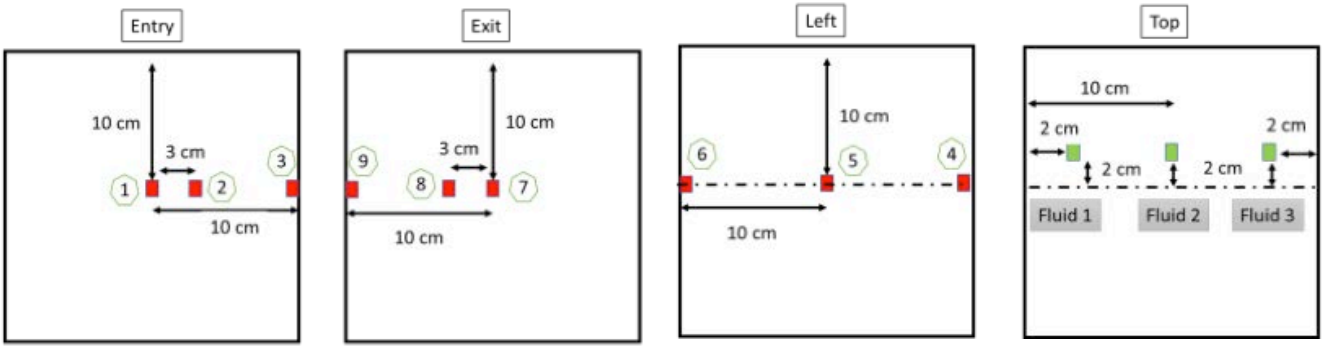

Figure 3 Location of Tracer Elements

Table 2 Summary of Material Properties and Constitutive Model

Property	Tank	Fluid
Density (kg/m^3)	2,700	1,000
Elastic Modulus (GPa)	70	N.A.
Bulk Modulus (GPa)	N.A.	2.2
Von Mises Yield Strength (GPa)	20	N.A.
Mass (kg)	N.A.	N.A.
Thickness (mm)	2.0	N.A.
Poisson Ratio	0.33	N.A.

velocity, and effective stress were taken from the nodes and elements output at the center of each wall. The gauges corresponded to shell element gauge no. 1, 5, and 7 (as shown in Figure 3). Similarly, the fluid pressures generated during the shock and drag phase were plotted using data collected from fluid gauge no. 2.

Baseline Model 1

The baseline Model 1 simulation was set up for a 100%-water-filled tank impacted without penetration at the center of the entry wall by a spherical rigid projectile with an initial velocity of 300 m/s. Even though this is a hypothetical situation, because the projectile would likely penetrate the entry wall in an actual experiment, this simulation provided some insight to the tank wall behavior during the initial shock phase of the HRAM event. The event was simulated for 1 ms with a sampling rate of 20 µs for data collection. For comparison purposes, the following discussion compares Model 1 to an empty tank impacted under the same conditions.

Entry wall X-displacement and X-velocity plots are shown in Figures 4 and 5, respectively. The X-direction corresponds to the major component of the entry wall, as the direction of projectile velocity impacting the entry wall is in the positive X-direction.

It was observed the peak displacement of the entry wall for the 100%-filled baseline Model 1 is higher at around 9 mm as compared to 7 mm for the empty tank. An interesting phenomenon observed for Model 1 was the entry wall displacing in the negative X-direction at around 0.06 ms after impact, indicating the entry wall bulging outward. The X-component velocity time-history plot shown in Figure 5 indicates a much larger peak value of around 210 m/s in the negative X direction right after projectile impact.

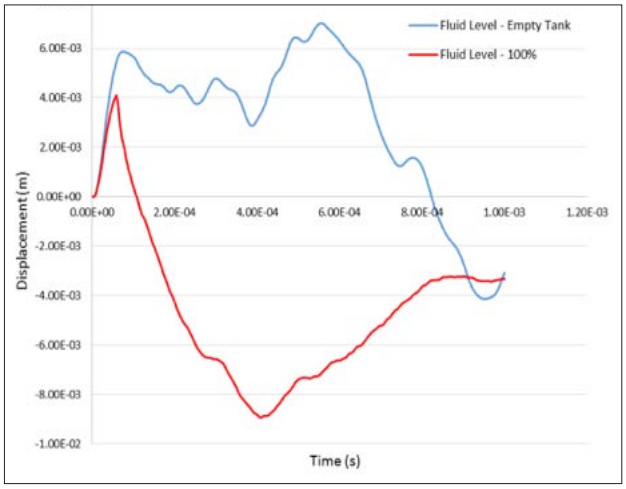

Figure 4 (left) Entry Wall X-Displacement for Model 1

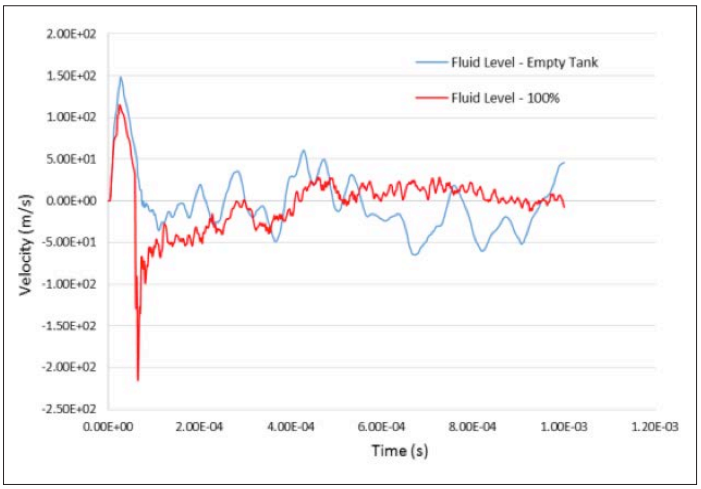

Figure 5 (right) Entry Wall X-Velocity for Model 1

This result corresponds to the time when the entry wall starts to bulge. The subsequent velocity of the entry wall after deforming outward was lower compared to the empty tank. The effective entry wall stress (i.e., the von Mises stress) reached a 11% higher peak value for Model 1 but over a shorter duration of time than the empty tank.

The exit wall response to HRAM is of main interest in this study as it is an area on the aircraft where main structural components and load-bearing members are likely to be located. Graphs for exit wall response were plotted from data collected from the center node of the exit wall panel. The X-displacement plot in Figure 6 shows a peak displacement of around 2 mm experienced by the exit wall at the end of the simulation, a value which is much higher than was experienced by the empty tank. The exit wall for Model 1 started deforming earlier at approximately 0.13 ms. This is approximately the time where the initial shock wave due to projectile impact at the entry wall impinged onto the exit wall, causing it to displace. The presence of fluid in the tank actually resulted in a much smaller velocity and effective stress at the exit wall. Peak stress at the center of the exit wall registered a much lower value of approximately 100 MPa, as compared to 500 MPa for the empty tank.

Besides the propagation of shock wave through the aluminum tank structure, a hemispherical shock wave was observed to propagate in the fluid toward the exit wall. This ram pressure generated by the impact of the projectile in the shock phase was recorded by the three fluid tracer elements, whose locations are shown in Figure 3.

Data for the ram pressure collected by the fluid element pressure tracer are plotted in Figure 7 (with the inset figure showing the fluid gauge locations). The graph showed a peak pressure of 7 MPa, as recorded by fluid gauge 1, which is located nearest to the impact point. This ram pressure was found to weaken significantly as it propagated through the fluid medium, reducing to a magnitude of 0.9 MPa near the exit wall, as recorded by fluid gauge 3. As the shock wave moved across the fluid toward the exit wall, its energy was dissipated across a larger volume of fluid, thereby resulting in a drastic reduction in ram pressure. The rapid weakening of the initial shock wave due to geometric expansion about the impact point and its short duration indicated the left and exit walls of the tank are unlikely to experience significant pressures from the impact shock wave.

The simulation for baseline Model 2 was set up for a 2-mm-thick 100%-water-filled tank, with the initial position of the spherical projectile centered and flushed to the inner surface of the entry wall and given an initial velocity of 250 m/s. Model 2 was developed to assist in understanding the structural response of the tank walls during the drag and cavitation phase of HRAM. All displacement, velocity, and effective

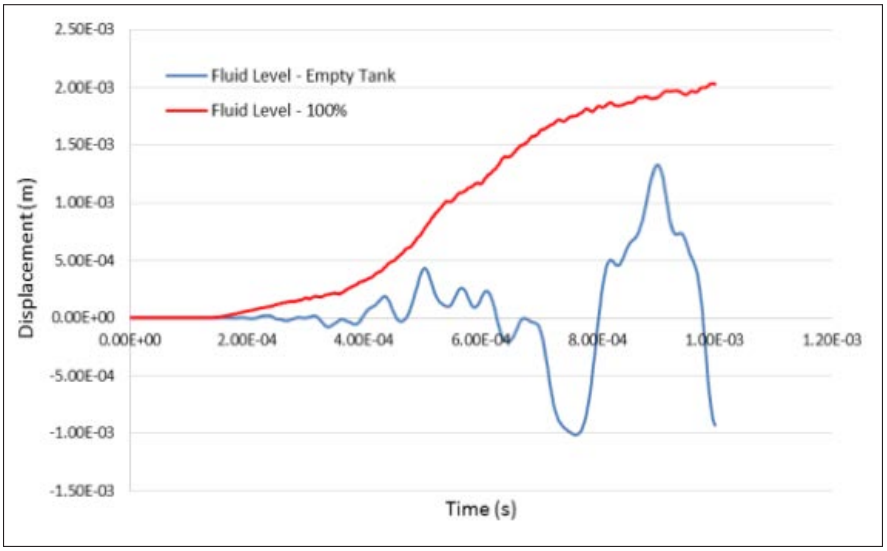

Figure 6 Exit Wall X-Displacement for Model 1

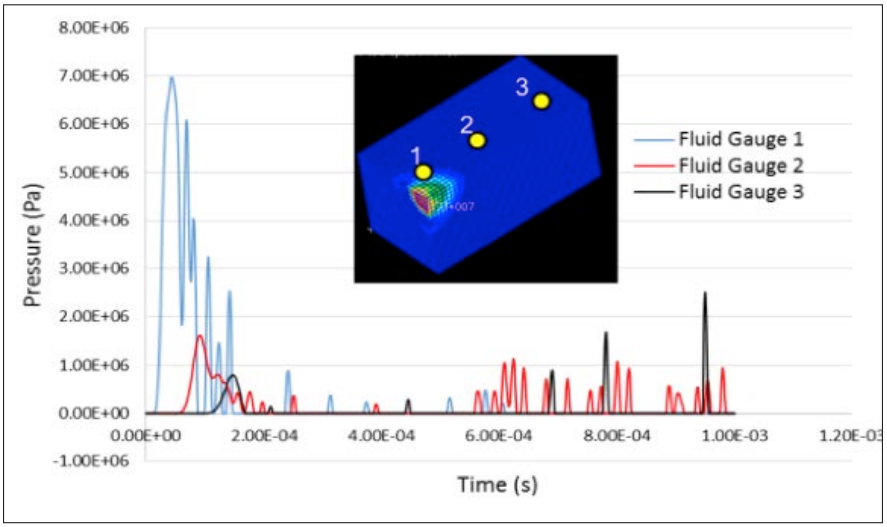

Figure 7 (Shock Pressure Generated by a 300-m/s Spherical Projectile for Model 1

stress values plotted were obtained from the center node or element of the tank walls. Because the collapse of the cavity would most likely occur at a much later time, the cavitation collapse pressure and its subsequent effect on the tank walls were omitted from this study. Instead, the effects on tank walls due to the drag phase pressure and the formation of the cavity in the fluid were the main interest.

The exit wall response graphs were plotted from the start of simulation up to 1.5 ms, just before the projectile impacted the exit wall. The exit wall started to move and deform at approximately 0.13 ms into the simulation due to the initial shock wave impinging onto the exit wall. At approximately 1 ms into the simulation, the rate of displacement of the exit wall registered an increase, as observed from the steeper gradient of the displacement time-history plot of the exit wall. Correspondingly, there was a sharp increase in the exit wall X velocity after 1 ms, as illustrated in Figure 8. This increase is due to the projectile approaching the exit wall and the high-pressure region in front of the projectile during the drag phase, exerting a greater pressure on and prestressing the exit wall before projectile impact.

The prestressing of the exit wall before the projectile impact is further illustrated in Figure 9. Likewise for the exit wall velocity, the effective stress has the peak value after 1 ms, when the projectile approached the exit wall. The exit wall registered a peak velocity of 7 m/s and a peak stress of approximately 94 MPa prior to projectile impact.

Figure 10 shows the drag phase fluid pressure recorded by fluid gauge 2,

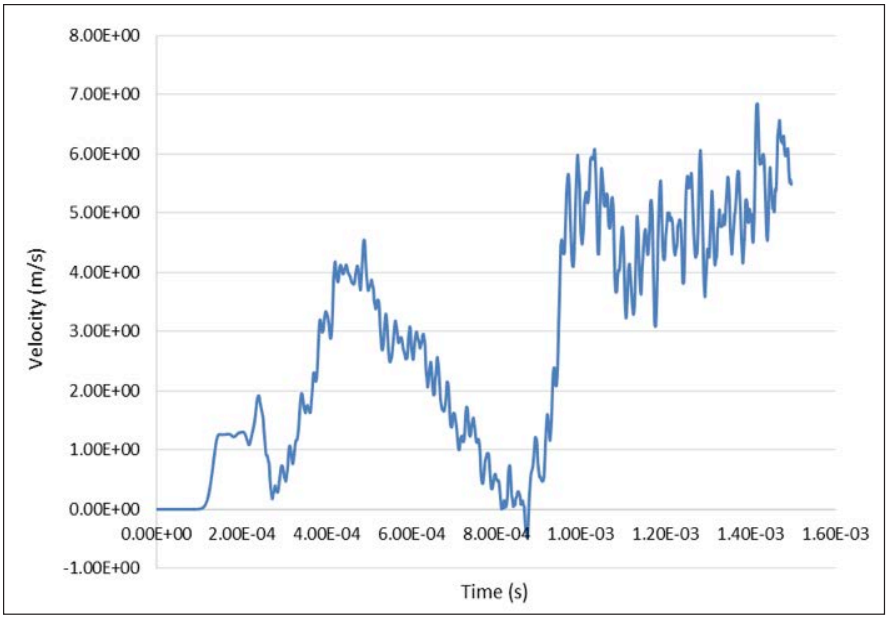

Figure 8 Exit Wall X-Velocity for Model 2

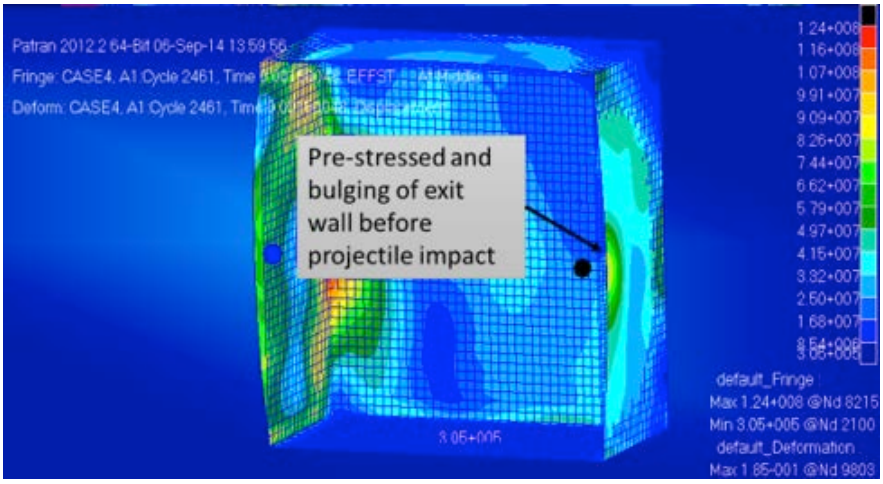

Figure 9 Effective Stress Fringe Plot Showing Prestressed Exit Wall During the Drag Phase for Model 2

located in the middle of the tank near the shotline. A peak pressure of approximately 5 MPa was registered as the projectile approached fluid gauge 2 at around 0.5 ms. The drag phase pressure rise was gradual and occurred over a longer period of time, as compared to the initial shock phase pressure. As the projectile moved past fluid gauge 2, the pressure recorded went to 0, indicating the formation of a cavity behind the projectile path. The cavitation phase of HRAM, which includes the oscillation and the subsequent collapse of the cavity, is not part of this study, as it would occur after the simulation had ended.

An interesting parameter that the numerical simulation provided for drag phase analysis was the cavity evolution when the projectile traverses the fluid towards the exit wall. The Model 2 simulation fringe plot of material fraction in the fluid Euler mesh obtained at a 0.4-ms interval is shown in Figure 11. The maximum cavity diameter measured from the fringe plot at 2 ms was found to be approximately 60 mm. The bulging of the entry and exit wall was also observed.

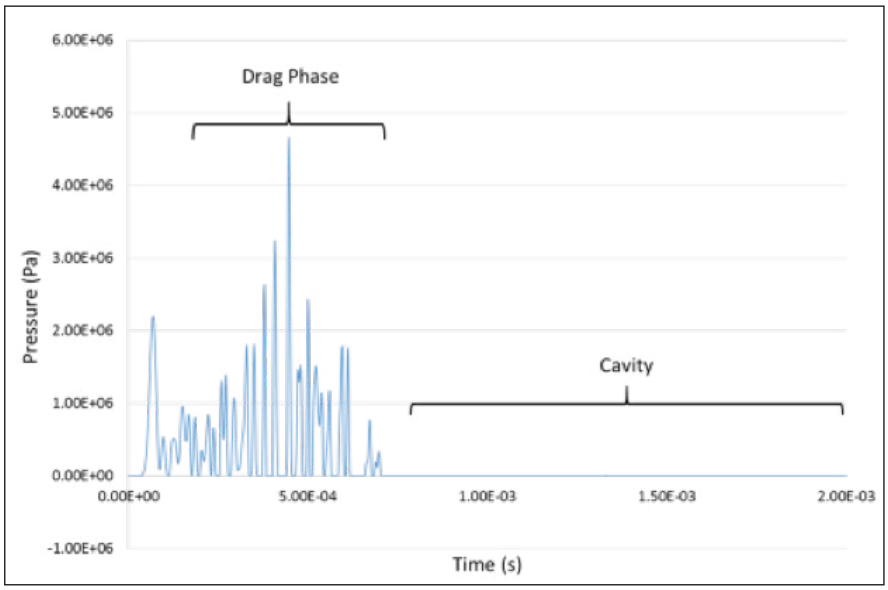

Figure 10 Drag Phase Fluid Pressure Output From Fluid Gauge 2 (Model 2)

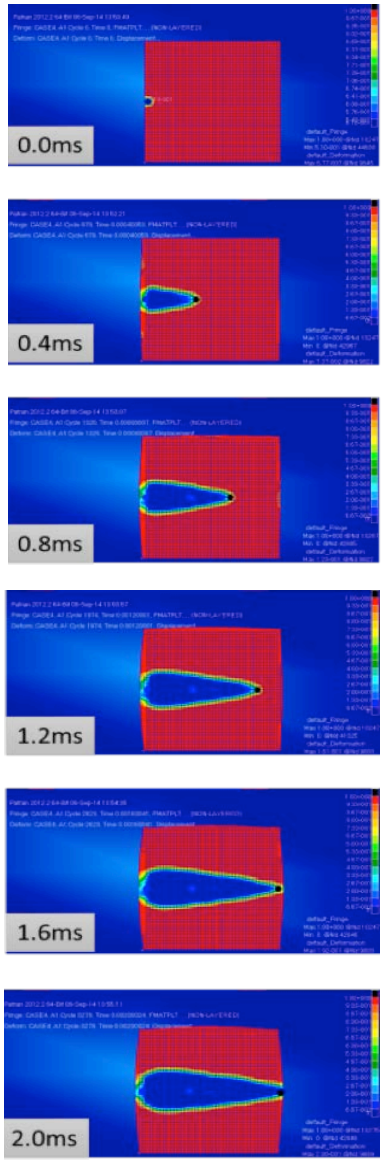

Figure 11 Cavity Evolution in Model 2

Parametric Studies Conducted for Model 1 and Model 2

Parametric studies were conducted on Model 1 and 2 to understand how different factors could affect the exit wall response. For Model 2, even though the simulation end time was set at 2 ms, peak values that were tabulated were chosen from the start of simulation until the point before the projectile impacted the exit wall.

The fluid level was varied for Model 1 and 2 to study the effects of free surface on the shockwave propagation and the resultant exit wall response. With the rest of the parameters and impact conditions kept constant, the fluid level was varied for 80% and 60% fluid levels. This variation was made possible by adjusting the initial condition of the fluid elements filling the tank.

The exit wall response and fluid pressures for Model 1 and Model 2 are tabulated in Table 3 and Table 4, respectively. For Model 1, it was observed the lower fluid levels resulted in a lower exit wall displacement but higher velocity and stress. The shock phase ram pressure was also reduced significantly from 1.61 MPa in the fully filled tank to a mere 0.45 MPa in the 60%-filled tank. This was due to the presence of free surface distorting the hemispherical formation of the shock wave at the impact point.

The reduction of exit wall displacement is more evident in Model 2 from 4.7 mm for the fully filled tank to 2.7 mm for the 60%-filled tank. The peak stress at the

Table 3 Model 1 Exit Wall Response to Varying Fluid Levels

Parameters	Percent-Filled Level	Maximum Displacement (m)	Peak Stress (MPa)	Shock Phase Ram Pressure From Fluid Guage 2 (MPa)	Peak Velocity (m/s)
Fluid Level Variation	100	0.002035	104.802	1.61365	12.7263
	80	0.002027	170.765	1.3469	19.1264
	60	0.001714	240.244	0.45185	19.2642

Table 4 Model 2 Exit Wall Response to Varying Fluid Levels

Parameters	Percent-Filled Level	Maximum Displacement (m)	Peak Stress (MPa)	Peak Fluid Drag Pressure From Fluid Gauge 2 (MPa)	Peak Velocity (m/s)
Fluid Level Variation	100	0.00471648	94.074	4.64315	6.85024
	80	0.00398923	102.79	4.27619	6.23109
	60	0.00274174	109.94	3.0948	4.98805

exit wall for the three different fluid levels shows a lesser variation as compared to Model 1. Peak drag phase pressure was also observed to be higher for a 100%-filled tank at 4.63 MPa compared to 3.09 MPa for a 60%-filled level.

Projectile mass was varied from 2 g to 6 g. Results are tabulated in Tables 5 and 6. Model 1 results showed projectile mass having a strong effect on the exit wall response during the initial shock phase. Peak displacement, stress, velocity, and ram pressures were all found to increase significantly. By increasing the mass from 4 g to 6 g, the peak stress recorded a considerable increase from 105 MPa to 172 MPa.

However, for Model 2, the variation in projectile mass on exit wall response was not proportional to the mass. The peak fluid drag pressure was also found to be of similar magnitude for the 4-g and 6-g projectile. Nevertheless, some correlation was observed for the peak stress and velocity at the exit wall for Model 2, where a higher projectile mass resulted in a higher peak stress and velocity.

The initial velocity of the projectile was also varied from 100 m/s to 500 m/s. The results for Model 1 and 2 exit wall response are tabulated in Tables 7 and 8, respectively. Model 1 results indicated a strong influence of projectile velocity on the exit wall response and fluid ram pressures. A projectile impacting the tank at a higher velocity of 500 m/s resulted in a drastic increase in peak stress and velocity at the exit wall. The ram pressure from projectile impact saw an increase from 1.61 MPa for the baseline Model to 2.39 MPa for a 500-m/s projectile.

Table 5 Model 1 Exit Wall Response to Varying Projectile Mass

Parameters	Mass (g)	Maximum Displacement (m)	Peak Stress (MPa)	Shock Phase Ram Pressure From Fluid Guage 2 (MPa)	Peak Velocity (m/s)
Projectile Mass	2	0.00128098	70.5868	1.0475	7.32631
	4	0.00203513	104.802	1.61365	12.7263
	6	0.00243127	172.462	2.02303	16.4221

Table 6 Model 2 Exit Wall Response to Varying Projectile Mass

Parameters	Mass	Maximum Displacement (m)	Peak Stress (MPa)	Peak Fluid Drag Pressure From Fluid Gauge 2 (MPa)	Peak Velocity (m/s)
Projectile Mass	2	0.00295588	68.2312	2.68013	4.07203
	4	0.00471648	125.866	4.64315	8.3379
	6	0.00478961	170.508	4.52462	13.4958

Table 7 Model 1 Exit Wall Response to Varying Projectile Initial Velocity

Parameters	Projectile Velocity (m/s)	Maximum Displacement (m)	Peak Stress (MPa)	Shock phase Ram Pressure From Fluid Gauge 2 (MPa)	Peak Velocity (m/s)
Projectile Velocity	100	0.000660054	29.5669	0.46631	2.78716
	300	0.00203509	104.802	1.61365	12.7263
	500	0.00255664	406.831	2.39176	34.2576

Table 8 Model 2 Exit Wall Response to Varying Projectile Initial Velocity

Parameters	Projectile Velocity (m/s)	Maximum Displacement (m)	Peak Stress (MPa)	Peak Fluid Drag Pressure From Fluid Gauge 2 (MPa)	Peak Velocity (m/s)
Projectile Velocity	100	0.00123423	32.48	2.72262	1.61611
	250	0.00471674	125.866	4.64315	8.3379
	500	0.00589209	157.726	10.6443	20.3856

It was evident the exit wall response and fluid pressure were even more sensitive to projectile velocity for Model 2. With an increase in velocity from 250 m/s to 500 m/s, the displacement of the exit wall saw an increase from 4.72 mm to 5.89 mm. Similarly, as shown in Figure 12, drag phase pressure doubled due to the projectile velocity increasing from 250 m/s to 500 m/s.

The elastic modulus of the tank material was varied from 40 GPa to 70 GPa, while keeping the rest of the parameters constant. Examination of the data presented in Table 9 revealed no particular trend for displacement and velocity for the different elastic modulus. However, there was a noticeable trend for both displacement and velocity for the variation in elastic modulus shown in Table 10.

The X-displacement plot for the exit wall showed the 100 GPa tank had a larger displacement initially but was eventually

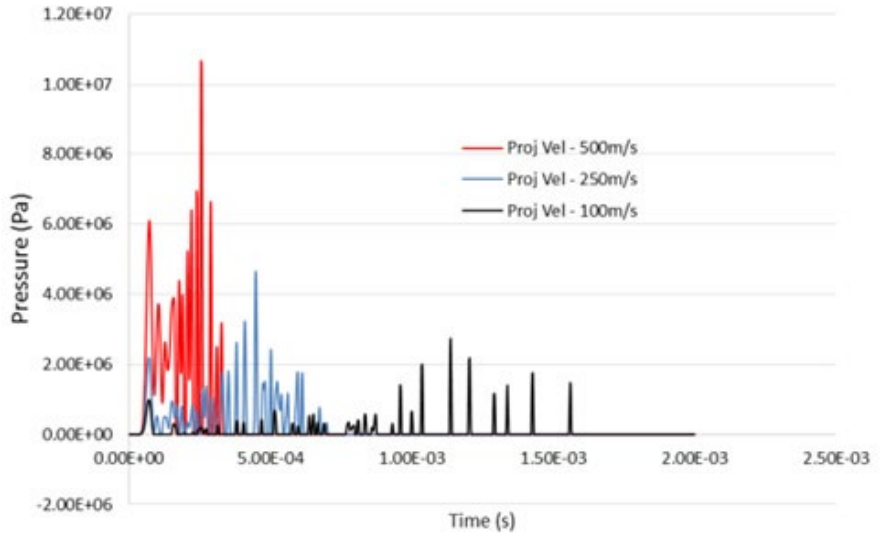

Figure 12 Drag Phase Pressure for Different Projectile Velocities (Model 2)

Table 9 Model 1 Exit Wall Response for Varying Tank Material Modulus

Parameters	Elastic Modulus (GPa)	Maximum Displacement (m)	Peak Stress (MPa)	Shock Phase Ram Pressure From Fluid Gauge 2 (MPa)	Peak Velocity (m/s)
Tank Material Modulus	40	0.00180311	72.9672	1.04987	11.6687
	70	0.00203509	104.802	1.61365	12.7263
	100	0.00181285	142.944	2.0287	9.30065

Table 10 Model 2 Exit Wall Response for Varying Tank Material Modulus

Parameters	Elastic Modulus (GPa)	Maximum Displacement (m)	Peak Stress (MPa)	Peak Fluid Drag Pressure From Fluid Gauge 2 (MPa)	Peak Velocity (m/s)
Tank Material Modulus	40	0.00502539	73.4471	5.35703	9.39117
	70	0.00471648	125.866	4.64315	8.3379
	100	0.00435498	152.739	3.00561	7.25874

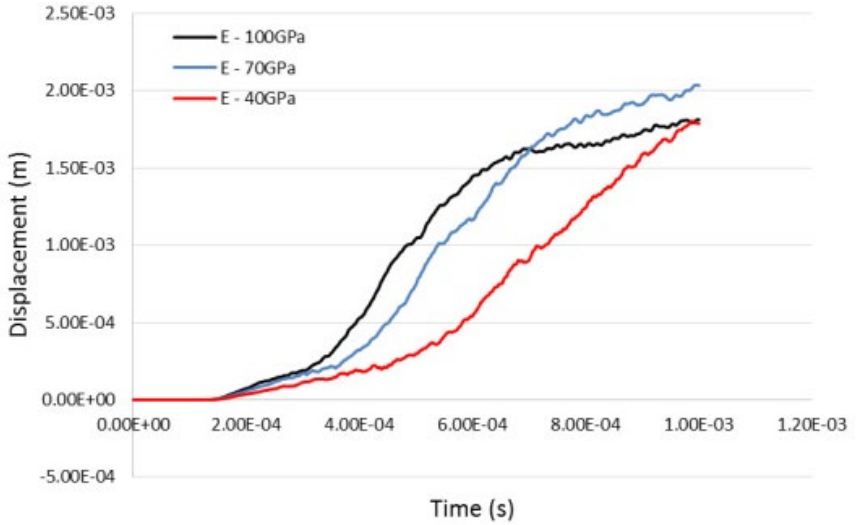

Figure 13 Exit Wall X-Displacement for Different Elastic Modulus (Model 1)

overtaken by tanks with lower modulus, as seen in Figure 13. This is an interesting phenomenon, which warrants further investigation. Values for peak stress and shock phase ram pressure for Model 1 did see a correlation, with the stiffer tank with modulus of 100 GPa experiencing a higher stress and larger ram pressure at 143 MPa and 2.03 MPa, respectively.

Moving to Model 2, the effect of varying Young's modulus was minimal for the exit wall displacement and velocity. However, the correlations for peak stress and drag phase pressures were more apparent, with the stiffer tank experiencing a larger stress but smaller drag pressures.

The next parametric study conducted on Model 1 and 2 was the variation in the density of the tank's material. With the baseline Model 1 and 2 having the density of 2,700 kg/m^3, material density was changed to 1,500 kg/m^3 and 4,500 kg/m^3 to evaluate its effect on the structural response at the exit wall. The results obtained are summarized in Tables 11 and 12.

Data from Table 11 indicated no discernible effect of material density on displacement and stress. It was observed that the baseline Model 1 has the highest displacement and stress, but the difference in value for the different material density was small. Some correlations were observed for shock ram pressure and velocity, with the denser material at 4,500 kg/m^3 having a smaller ram pressure of 1.09 MPa and peak velocity of 10.7 m/s. For Model 2, the simulation model found that varying material density has almost negligible effects on the exit wall displacement. Peak stress and velocity also see small changes even though density was varied from 1,500 kg/m^3 to 4,500 kg/m^3.

For the final investigative choice, the density of the fluid was varied from 800 kg/m^3 to 1,200 kg/m^3, with the baseline Model 1 and 2 having the density of water at 1,000 kg/m^3. Results for this study are tabulated in Tables 13 and 14.

The effect of fluid density on the shock phase of the HRAM for Model 1 saw no consistent trend at the exit wall, especially for stress, velocity, and ram pressure. Even though displacement of the exit wall for lower fluid density seemed to be higher, the difference is perceived to be small. Results for shock phase ram pressure were also inconsistent, with the more dense and less dense fluids both having a smaller ram pressure than the baseline Model 1.

As for the drag phase analysis for Model 2, varying fluid density was observed to have little effect on the exit wall displacement. However, the less dense fluid allowed the projectile to reach the exit wall earlier. With lower fluid density of 800 kg/m^3, the projectile reached the exit wall after 1.4 ms, approximately 0.5 ms faster than the denser fluid with a density of 1,200 kg/m^3.

Table 11 Model 1 Exit Wall Response for Varying Tank Material Density

Parameters	Density (kg/m^3)	Maximum Displacement (m)	Peak Stress (MPa)	Shock Phase Ram Pressure From Fluid Gauge 2 (MPa)	Peak Velocity (m/s)
Tank Material Density	1,500	0.00187647	93.5504	2.08677	13.448
	2,700	0.00203509	104.802	1.61365	12.7263
	4,500	0.00151676	98.4064	1.08979	10.6776

Table 12 Model 2 Exit Wall Response for Varying Tank Material Density

Parameters	Density (kg/m^3)	Maximum Displacement (m)	Peak Stress (MPa)	Peak Fluid Drag Pressure From Fluid Gauge 2 (MPa)	Peak Velocity (m/s)
Tank Material Density	1,500	0.00466953	124.526	4.70424	9.52921
	2,700	0.00471648	125.866	4.64315	8.3379
	4,500	0.00465953	109.789	5.27148	7.03468

Table 13 Model 1 Exit Wall Response to Varying Fluid Density

Parameters	Density (kg/m^3)	Maximum Displacement (m)	Peak Stress (MPa)	Shock Phase Ram Pressure From Fluid Gauge 2 (MPa)	Peak Velocity (m/s)
Fluid Density	800	0.00208119	126.662	1.16409	14.1915
	1,000	0.00203512	104.802	1.61365	12.7263
	1,200	0.00178056	105.41	1.5171	14.2918

Table 14 Model 2 Exit Wall Response to Varying Fluid Density

Parameters	Density (kg/m^3)	Maximum Displacement (m)	Peak Stress (MPa)	Peak Fluid Drag Pressure From Fluid Gauge 2 (MPa)	Peak Velocity (m/s)
Fluid Density	800	0.00463453	129.618	3.99885	10.0071
	1,000	0.00471674	125.866	4.64315	8.3379
	1,200	0.00475732	142.476	5.35016	13.8578

CONCLUSIONS

HRAM is a complex phenomenon that is still not well understood. However, computational models can now provide an alternative to experimental testing in the understanding of HRAM by coupling the tank mesh to fluid mesh to simulate the fluid structure interaction. In particular, FE Models 1 and 2 provided some insights into the dynamic response of the tank structure and fluid pressures at the early phases of the HRAM phenomenon.

For the studies conducted with Models 1 and 2, the examination and analysis of the data collected revealed the following observations.

- The initial shock wave pressure upon projectile impact is unlikely to have detrimental effects on the exit wall of tank due to its rapid extinction in the fluid.
- The presence of free surface with lower filling levels reduced both the initial shock pressure and subsequent drag phase pressures.
- The projectile mass has a strong effect on the exit wall response during the shock phase, but once the projectile penetrates the entry wall, the drag phase was not correlated to different projectile masses.
- The velocity of the projectile had the largest influence on the exit wall response and fluid pressures, as the kinetic energy of the projectile is proportional to the square of its velocity. Therefore, when projectile velocity was increased to 500 m/s, all data collected for analysis observed a

huge increase, especially during the drag phase.

- The tank material with a higher Young's modulus resulted in a larger shock pressure but smaller drag phase pressures.
- Effective stress experienced by the exit wall was significantly greater for the stiffer tank.
- Varying tank material density had little effect on the exit wall response during the drag phase.
- Increasing the density of fluid in the tank resulted in higher drag phase pressures.
- As expected, the projectile was observed to reach the exit wall at a later time with increased fluid density. ASJ

ABOUT THE AUTHORS

Mr. Kangjie (Roy) Yang is a mechanical engineer at Singapore Technologies (ST) Aerospace Limited, where he supports the Engineering and Development Centre's (EDC's) work on military projects and the Republic of Singapore's Air Force fleet of aircraft. He holds a degree in mechanical engineering (majoring in aeronautical engineering) from Nanyang Technological University and is pursuing postgraduate studies at the National University of Singapore and Naval Postgraduate School.

Dr. Young W. Kwon is a Distinguished Professor in the Mechanical and Aeronautical Engineering Department of the Naval Postgraduate School. His research interests include multi-scale and multi-physics computational techniques for material behaviors, composite materials, fracture and damage mechanics, nanotechnology, and biomechanics. He has authored or co-authored more than 300 technical publications, including textbooks on FE methods using MATLAB and multiphysics and multiscale modeling. He is an ASME fellow and is the Technical Editor of the ASME *Journal of Pressure Vessel Technology* as well as the *Journal of Materials Sciences and Applications*. He holds a Ph.D. from Rice University.

Mr. Christopher Adams is the Director of the Center for Survivability and Lethality at the Naval Postgraduate School, where he currently teaches combat survivability. He is a former Associate Dean of the Graduate School of Engineering and Applied Sciences, as well as a former thesis student of Distinguished Professor Emeritus Robert Ball. He also accumulated more than 20 years of operational flight experience in F-14s and EA-6Bs, serving multiple tours in Iraq and Afghanistan. Mr. Adams holds a B.S. degree in aerospace engineering from Boston University and an M.S. degree in aerospace engineering from the Naval Postgraduate School.

Maj. Dave Liu is an assistant professor of Aeronautical and Astronautical Engineering at the Air Force Institute of Technology (AFIT), leading the school's aircraft combat survivability education and research program. Prior to this experience, he was deployed as a member of the Joint Combat Assessment Team in Afghanistan, where he collected aircraft combat damage data for U.S. and coalition air assets.

References

[1] Kimsey, K. D. "Numerical Simulation of Hydrodynamic Ram." ARBRL-TR-02217, U.S. Army Ballistic Research Laboratory, Aberdeen Proving Ground, MD, February 1980.

[2] Varas, D., J. López-Puente, and R. Zaera. "Experimental Analysis of Fluid-Filled Aluminium Tubes Subjected to High-Velocity Impact." *International Journal of Impact Engineering*, vol. 36, pp. 81–91, 2009.

[3] Bestard, J., M. Buck, B. Kocher, and J. Murphy. "Hydrodynamic Ram Model Development – Survivability Analysis Requirements." 53rd AIAA/ASME/ASCE/AHS/ASC Structures, Structural Dynamics and Materials Conference, 20th AIAA/ASME/AHS Adaptive Structures Conference 14th AIAA, 2012.

[4] MSC Software Corporation. Dytran *2010 Theory Manual.* Santa Ana, CA, 2010.

[5] Ball, R. E. *The Fundamentals of Aircraft Combat Survivability Analysis and Design.* Second edition, Reston, AIAA, pp. 328–330, 2003.

[6] Bharatram, G., S. Schimmels, and V. Venkayya. "Application of MSC/DYTRAN to the Hydrodynamic Ram Problem." MSC User's Conference, Universal City, CA, pp. 13–16, 1995.

DSIAC HEADQUARTERS
4695 MILLENNIUM DRIVE
BELCAMP, MD 21017-1505

CALENDAR OF EVENTS

SEPTEMBER

JAS Program Review
20–22 September
West Palm Beach, FL

2016 MSS EO & IRCM Conference
27–29 September
Gaithersburg, MD
https://www.sensiac.org

OCTOBER

8th Triennial International Fire & Cabin Safety Research Conference
24–27 October
Atlantic City, NJ
http://www.fire.tc.faa.gov/2016Conference/conference.asp

Precision Strike Association Symposium
25–27 October
Laurel, MD
http://www.precisionstrike.org/events/7PST/7PST.html

NOVEMBER

Rotocraft Virtual Engineering Conference
8–9 November
University of Liverpool, UK
http://www.vtol.org/events/rotocraft-virtual-engineering-conference

Aircraft Survivability Symposium
8–10 November
Monterey, CA
http://www.ndia.org/meetings/7940/Pages/default.aspx

Aircraft Survivability Equipment Symposium
14–16 November
Huntsville, AL
http://www.quad-a.org/

Information for inclusion in the Calendar of Events may be sent to:

DSIAC Headquarters
4695 Millennium Drive
Belcamp, MD 21017-1505

Phone: 443/360-4600
Fax: 410/272-6763
Email: *contact@dsiac.org*

To update your mailing address, fax a copy of this page with changes to 410/272-6763 or scan and email it to contact@dsiac.org.